Turkish Journal of Civil Engineering, 2025, xxxx-xxxx, Paper xxx, ***Research Article***

Utilization of Artificially Cemented Sand for Porous Pavement Applications and Analysis of Runoff Control

Israf JAVED[1]
Abdullah EKINCI[2*]
Bertuğ AKINTUĞ[3]

ABSTRACT

This study investigates the effects of curing period (0, 4, 7, and 28 days), density (1.6 and 1.8 g/cm³), and cement content (1%, 3%, 6%, and 10%) on the behavior of cemented sand. Unconfined compressive strength (UCS) tests assessed strength, while permeability was evaluated through constant head tests. Additionally, ultra-pulse velocity (UPV) testing was used to assess shear modulus (G_0) as a nondestructive evaluation method. The findings demonstrate that increasing the cement content and extending the curing duration enhance both strength and shear modulus while reducing permeability. Specifically, a cement content of 10% and a curing period of 28 days result in a significant improvement, with UCS reaching 2.7 MPa and G_0 attaining 1.2 MPa. Higher density also enhances strength and G_0 but lowers permeability. Hydrological modeling of stormwater systems reveals that increasing cement content elevates surface runoff volume and shifts the soil Curve Number from 61 to 89 (for 1% and 10% cement at 1.8 g/cm³ density, respectively), indicating reduced infiltration capacity and increased runoff potential. Statistical analysis confirmed significant relationships between cement content, curing time, density, and the resulting strength and permeability, with p-values below 5%, indicating strong statistical significance. For urban stormwater systems requiring permeability-strength equilibrium, the 1.8 g/cm³ density, 6% cement, and 7-day curing mix is recommended to support groundwater recharge while maintaining pavement durability.

Keywords: Cemented sand, strength, permeability, pavement, LID, curve number.

Note:

- This paper was received on December 18, 2024 and accepted for publication by the Editorial Board on May 2, 2025.
- Discussions on this paper will be accepted by xxxxxxx xx, xxxx.

• https://doi.org/

1 Middle East Technical University, Civil Engineering Program, Northern Cyprus Campus, Guzelyurt, Turkish Republic of Northern Cyprus
israf.javed@metu.edu.tr - https://orcid.org/0000-0003-4323-6892

2 Middle East Technical University, Civil Engineering Program, Northern Cyprus Campus, Guzelyurt, Turkish Republic of Northern Cyprus
ekincia@metu.edu.tr - https://orcid.org/0000-0002-6787-9983

3 Middle East Technical University, Civil Engineering Program, Northern Cyprus Campus, Guzelyurt, Turkish Republic of Northern Cyprus
bertug@metu.edu.tr - https://orcid.org/0000-0001-6206-4315

* Corresponding author

PREPRINT

1. INTRODUCTION

Sandy soils are abundant worldwide and have become more prevalent in construction projects due to rapid development, covering approximately 4.99×10^9 hectares, which represents about 31% of the Earth's total land area. These soils are predominantly formed in glacial or alluvial deposits. They are also found in inland regions, particularly in arid and semi-arid areas such as the Sahara Desert, Saudi Arabia, Turkey, northwestern China, and western Australia [1]. Nevertheless, the utilization of sandy soils in structures presents various challenges, including rapid infiltration and conductivity, high settlement, liquefaction, and low ability to hold water [2,3]. To overcome this challenge and ensure stability, innovative ground improvement technologies are necessary for its stabilization [4]. The concept of soil stabilization has a long history dating back 5000 years [5]. The ancient civilizations, such as at Egypt and Mesopotamia, employed stabilized earth roads. Lime was commonly used as a stabilizer by the Greeks and Romans to enhance the performance of their construction materials [6–8]. Today, the traditional approach to soil stabilization involves replacing unsuitable soil with stronger materials like gravelly soil, concrete, geogrids, and geotextiles [9,10]. While this method is effective, it is often associated with higher costs and longer implementation times due to the need for soil removal and replacement [11].

There are various new methods that are employed to enhance ground conditions for safe and reliable construction. These ground improvement techniques can be broadly classified into three categories based on the treatment method: mechanical, biological, and chemical stabilization [12,13]. Mechanical stabilization, the oldest known technique for ground improvement, can be traced back to ancient civilizations. By applying mechanical force and compacting the surface layers using static and dynamic loading, the density of the soil is increased, resulting in improved stability and load-bearing capacity [14,15]. Soil biological stabilization techniques involve the use of natural organisms and processes to improve the properties of soil [16],[17]. This approach is beneficial both for engineering purposes and for the environment, as it combines engineering practices with ecological principles to create a sustainable and eco-friendly solution [18]. Chemical stabilization modifies soil behavior by introducing additives that alter its physicochemical properties, enhancing geotechnical performance. Common agents include cementitious or pozzolanic materials like lime, cement, fly ash, and calcium-based compounds. These binders react with soil constituents, inducing processes such as cation exchange, flocculation, or pozzolanic reactions. The resulting structural changes improve shear strength, compressibility, and water resistance while minimizing volumetric instability [19–22]. These additives enhance the soil's strength and stability, making it suitable for construction purposes [23].

Chemical stabilization is a cornerstone of geotechnical engineering, employing binders such as Portland cement, lime, and fly ash to enhance soil properties [24–26]. These stabilizers are widely utilized in various countries for implementing soil chemical stabilization processes. Among these, Portland cement stabilization stands out for its global adoption and proven efficacy in improving mechanical performance, particularly in soils [27–29]. Cement stabilization works by inducing hydration reactions that form stable interparticle bonds, thereby increasing strength, durability, and load-bearing capacity [30]. Researchers worldwide have extensively explored this method, investigating variables such as cement content, curing conditions, and soil-cement interactions to optimize outcomes like unconfined compressive strength (UCS), shear strength parameters (cohesion, void ratio, and

PREPRINT

friction angle), permeability, compaction, and microstructure. As summarized in Table 1, these studies systematically evaluate diverse soil types, cement dosages, curing regimes, and their effects on measured geotechnical and microstructural properties.

Table 1 - Summary of Key Findings from Literature on Cemented Soil Behavior

Ref.	Soil Type	Cement Content	Curing Condition	Measured Properties	Main Findings
31	Clayey sand (SC)	OPC (Type III): 1,2,3,5,9,12%	7 days (humidity >95%)	UCS, stress-strain, porosity, Moisture	UCS increases with cement content.
					UCS increases exponentially with reduced porosity.
					Peak UCS at ~10% moisture; strength declines beyond this.
					Voids/cement ratio best strength predictor.
32	Poorly graded sand (SP)	Lime Portland Cement; 2.5,5,7.5%	7,14,28 days (room temp)	UCS, shear strength (c, φ), E_{50}	UCS increases linearly; higher cement leads to brittle failure
					Cohesion increases significantly more than the internal friction angle
					Moisture content decrease while dry density increased with cement.
33	Dune sand (SP)	OPC (2.5,5 &7.5%) Cement kiln dust (CKD,5,10 ,20%),	28 days (sealed curing)	UCS, permeability, SEM/XRD	For OPC, increasing cement from 2.5% to 7.5% tripled UCS
					Higher stabilizer content reduced permeability across all soils.
					Calcite formation with LSP and 2.5% OPC increased roughness, friction, and UCS.
34	Osorio sand	OPC III:(1,3,5,7 ,9) % dry soil mass	2, 7, 28 days at 23°C, >95% RH	UCS, porosity (η), voids/cement ratio (η/Cv)	UCS increases with higher cement content, lower porosity, and longer curing
					A dosage equation was developed for curing, cement, and porosity
35	Poorly graded silica sands (SP)	OPC:3, 6, 9%; gypsum: 2, 3, 6, 9%.	20°C, 85% RH; 7, 28, 90 days	G_{max}, q_{ucs}, void ratio	G_{max} can be estimated from q_{ucs} regardless of cement type/void ratio.
					q_a and G_{max} are higher for Portland cement than gypsum.
					q_a and G_{max} increase with higher cement content and lower void ratio.
36	Natural Desert Sand (NDS)	OPC (5%) + Fly Ash (0,3,5,7%)	7, 14, 28 days (room temp)	UCS, CBR, Compaction (MDD, OMC)	UCS increased from 0.88 MPa (untreated) to 4.74 MPa (28-day curing)
					CBR for treated soil improved as compare to untreated soil.
					MDD increased, while OMC content decreased with increasing cement & FA content.
37	Low-plastic silt (ML)	Limestone Powder, SP (0%, 10%, 20%, 30%, 40%, and 50%)	0, 7, 14, 28 days (room temp)	Atterberg's limits, UCS, CBR, Compaction (MDD, OMC) and Consolidation.	UCS increased with SP up to 30%, then declined, shifting failure from ductile to brittle
					CBR improved from 7% (untreated) to 37% with 30% SP.
					Atterberg's limits decreased significantly with SP.
					MDD increased up to 30% SP, then declined, while OMC decreased continuously.
					Void ratio and permeability decreased continuously as SP increased from 0 to 50%.

PRE-PRINT

38	Poorly graded sand (SP)	Gypsum, Lime, Calcite, Portland Cement (4% & 12%)	M1-M2: Stress,14h & 4d; M3-M5: No Stress,4d	Stress-strain behavior, Secant Young's modulus/Stiffness	Portland cement showed minimal sensitivity to preparation methods and curing conditions; gypsum, lime, calcite behavior varied significantly
					Specimens cured under stress (M1, M2) exhibited higher Stiffness than unstressed methods (M3–M5)
					Specimens with Portland cement showed the highest stiffness across all testing techniques.
39	Natural Desert Sand (NDS)	OPC (0,3,5,7%)	Cured for 7, 14, 28, 60, and 96	CBR, Permeability, UCS, cohesion and friction angle	UCS with OPC content (0.89 MPa at 3% vs. 3.35 MPa at 7% after 7 days).
					Permeability reduced from 8.63×10^{-5} (3% OPC) to 1.33×10^{-5} (7% OPC).
					Cohesion and friction angle increased with OPC.
					NDS stabilized with 7% OPC is viable for low-traffic road layers
40	Poorly graded sand (SP)	OPC (3,5,7%) +Silica Fume: 0%, 0.25%, 0.5%, 1%	Cured for 3, 7, 14, 28, 42, and 56(room temp)	Compaction (MDD, OMC), UCS, pH, Stiffness, Microstructure	UCS increased with cement and curing (e.g., 154 kPa at 3% (3 days) vs. 1361 kPa at 7% (56 days))
					Increasing cement content increased dry unit weight and reduced moisture content
					Stiffness increased with cement and curing (e.g., 19.7 MPa at 3% (3 days) vs. 103.4 MPa at 7% (56 days))
					Denser matrix, reduced porosity, and improved interfacial transition zone (ITZ) with silica fume
41	Native soil from riverbed (SW)	5%, 7.5%, 10%, and 12.5%	Curing: 7 & 28 days; F-T: 12 cycles (-23°C, 24h / 21°C, 24h).	Compaction (MDD, OMC), UCS, Permeability. Durability	Permeability dropped from 9.48×10^{-4} to 9.64×10^{-5} cm/s at 12.5% cement (14 days).
					MDD and OMC increased with cement
					UCS and stiffness increased with cement content
					Weight loss after 12 freeze-thaw cycles decreased as cement content increased from 5% to 12.5% across

Cement stabilization improves soil properties through a synergistic interplay of physicochemical reactions and microstructural reorganization, driven primarily by the hydration of cement and subsequent pozzolanic activity. When Portland cement is introduced to soil, its tricalcium silicate (C_3S) and dicalcium silicate (C_2S) compounds react with water, producing calcium silicate hydrate (C-S-H) and calcium aluminate hydrate (C-A-H) gels [42–44]. These gels act as cementitious binders, coating soil particles and bridging gaps between them to form a rigid, interconnected matrix. Concurrently, calcium hydroxide ($Ca\ (OH)_2$), a byproduct of hydration, reacts with silica or alumina in the soil through pozzolanic reactions, generating additional C-S-H gels that further densify the matrix [45,46].

Unconfined Compressive Strength (UCS) in cement-stabilized soils is profoundly influenced by cement content, curing duration, and curing conditions. The addition of small amounts of cement (up to 2%) modifies soil properties, though these changes remain relatively minor. However, substantial improvements occur with higher cement dosages, as increased binder content significantly enhances stiffness, peak strength, and brittleness, for instance, sand treated with 10% cement exhibits marked strength gains alongside a shift toward brittle failure [47] [48]. Studies demonstrate a proportional relationship between cement dosage and

PRE-PRINT

UCS, with even minimal additions (e.g., 2%) yielding measurable improvements (e.g., 155 kPa), while higher contents (4&6%) substantially enhance strength 296 and 444 kPa respectively [49]. For instance, increasing cement content from 3% to 5% elevates 7-day UCS from 0.6 MPa to 1.6 MPa, with further gains from 0.7 to 2.7 MPa observed at 28 days [50]. Curing time is critical for UCS as early stages (7,14 and 28 days) drive rapid strength development due to hydration, while prolonged curing (>100 days) yields incremental gains as pozzolanic reactions mature [51,52]. Oh et al. [53] highlighted the role of curing temperature, recommending a range of 5–25°C to optimize UCS in lightweight air-trapped soils (ATS), while avoiding detrimental volumetric changes. Huang and Airey [54] systematically investigated artificially cemented carbonate sand, varying dry unit weight (13,16&19 kN/m³) and gypsum cement content (5,10&20%). Their findings reveal that UCS and stiffness increase with both cementation and density, though the influence of cementation diminishes at higher densities. UCS in cemented soils is governed by porosity, cement content, and soil type. The porosity/cement index, defined by an exponential porosity/binder equation [31], predicts strength and stiffness by quantifying void reduction and cementation effects [34,35]. Soil gradation significantly influences UCS gains, as coarser or finer matrices alter bonding efficiency. Collectively, these findings highlight cement's efficacy in transforming soil into a durable, high-strength material for geotechnical applications.

Permeability in cement-stabilized soils is critically influenced by cement content, with its relationship to hydraulic conductivity governed by soil type and curing conditions. While the correlation between cement dosage and permeability reduction can follow linear or power-function trends depending on soil characteristics [55,56], a marked decline in permeability is typically observed beyond threshold cement contents. For instance, in clayey soils, permeability decreases substantially when cement exceeds 8% by dry weight, as hydration products fill both intra- and inter-aggregate pores, densifying the matrix [57]. Similarly, in sandy soils, permeability drops significantly at 10% cement content, beyond which further reductions are marginal due to pore-filling saturation [58,59]. Microstructural evolution underpins these trends, scanning electron microscopy (SEM) reveals that cement-treated soils develop smaller, uniformly distributed pores compared to untreated soils [60]. At lower cement contents (e.g., <8%), hydration products primarily occupy intra-aggregate voids, moderately reducing permeability. Higher dosages (>8%) extend this pore-filling to inter-aggregate spaces, yielding a denser, more homogeneous microstructure and a pronounced permeability decline [57,61]. Curing duration further amplifies these effects. Extended curing allows hydration products to mature, enhancing pore-blocking efficiency and reducing permeability over time [62]. Additionally, adequate cement content, combined with a longer curing time, can lead to reduced permeability in soil [63] Density also plays a pivotal role, as higher dry unit weight correlates strongly with permeability reduction. In pervious concrete, for example, increased density (lower void ratios) exhibits a robust inverse relationship with permeability (R^2=0.768) [64].

Enhancing the mechanical properties of sandy soils has garnered significant attention due to their suitability as permeable pavement bases, offering a sustainable solution to urban stormwater management challenges [65]. Rapid urbanization, driven by a projected global population surge to 9.7 billion by 2050 and 11.2 billion by 2100, with 68% residing in urban areas [66,67] With urban expansion, more surfaces like roads, sidewalks, buildings, and parking lots replace natural ground cover [68,69]. These surfaces disrupt natural hydrological processes by reducing infiltration, thereby reducing groundwater recharge and elevating

PREPRINT

surface runoff. Consequently, during rainfall events, a diminished proportion of water permeates the soil, while runoff volumes and peak flow rates intensify significantly [68–70]. For instance, a study demonstrated that increasing impervious area from 1% to 32% in a residential development lacking stormwater controls led to a 4.9% rise in runoff volume [71]. Addressing the compounding effects of urbanization and climate change necessitates the implementation of proactive adaptation measures, such as permeable pavements. Permeable pavements, recognized as a Best Management Practice (BMP) and Low Impact Development (LID) technique in the U.S., provide an effective countermeasure by mimicking natural infiltration [70–72]. These systems are particularly advantageous in low-traffic zones like parking lots and sidewalks [73]. Coastal areas with sandy soils and gentle slopes have demonstrated the highest success rates in implementing alternative pavement installations [74]. Sandy soils, characterized by large particles and interconnected pore spaces, inherently promote rapid water infiltration and runoff reduction, making them ideal substrates for such systems. By contrast, clayey soils, despite their pollutant-retention capacity via cation exchange, hinder infiltration due to fine-grained, low-permeability matrices [75].

Urban stormwater management in rapidly developing regions like Türkiye demands sustainable solutions that balance mechanical durability and hydraulic efficiency. While porous pavements utilizing cemented sand show promise, existing studies often isolate strength or permeability optimization, overlooking critical trade-offs under variable cement contents, curing periods, and densities. Additionally, the relationship between nondestructive evaluation methods (e.g., ultrasonic pulse velocity, UPV) and stormwater performance metrics (e.g., Curve Number) remains underexplored. This study addresses these gaps through a two-phase approach: first, conducting controlled laboratory experiments to evaluate how cement content (1%, 3%, 6%, and 10%), curing duration (0, 4, 7, and 28 days), and density (1.6&1.8 g/cm³) influence key parameters such as unconfined compressive strength (UCS), stiffness (G_0) and permeability of cemented sand. Subsequently, the laboratory-derived parameters (permeability and void ratio) are integrated into stormwater modeling simulations to quantify their impact on runoff dynamics and infiltration efficiency (e.g., CN values). By correlating experimental outcomes with hydraulic performance, this study identifies optimal cementation protocols that enhance structural resilience while maintaining balanced infiltration, thereby harmonizing geotechnical and hydrological requirements in urban areas.

2. METHODOLOGY

2.1. Material

This section presents the material properties of sand and cement used in this study, detailing their fundamental characteristics in accordance with relevant standards. Additionally, their influence on porous pavement applications is analyzed.

2.1.1. Sand

In this study, standard sand (TS EN 196-1) was used to compare and evaluate the properties and behavior of the cemented sand samples. The standard sand has well-characterized properties, such as a known particle size distribution (Figure 1), which can help to ensure

PREPRINT

that the artificial cemented sand samples are prepared and tested in a consistent manner. The effective sizes of the sand particles were determined and reported in Table 2, which provides values for D_{10}, D_{30}, D_{60}, Coefficient of Curvature (C_c) and Coefficient of Uniformity (C_u). The sand was classified as a well-graded sand with SW designation using Unified Soil Classification System (USCS). This is important because a well-graded sand can have better compaction, permeability, and shear strength characteristics than a poorly-graded sand. Furthermore, the fact that the sand particles were found to be angular is also significant. Angular particles can interlock with one another more tightly, leading to increased friction and shear resistance. The specific gravity of the sand was found to be 2.62. The density of the sand can affect its ability to support loads and resist deformation, and it can also impact its porosity, permeability, and other important properties.

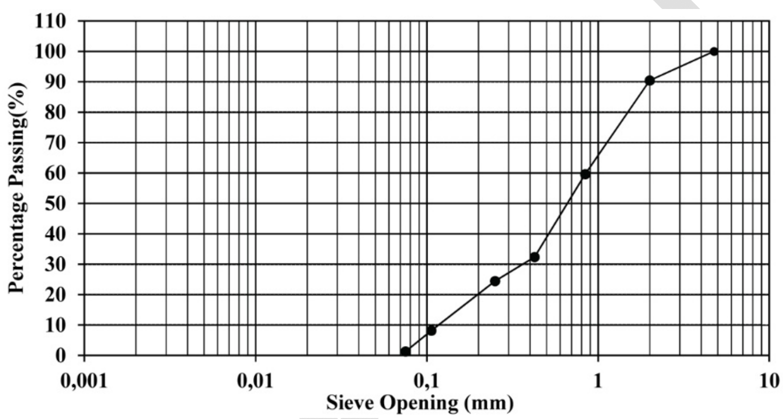

Figure 1 - Particle size distribution of sand

Table 2 - Physical properties of sand

Properties	Value
Specific Gravity	2.62
Gravel (4.75 mm < d) (%)	0.02
Sand (0.425 mm < d < 4.75 mm) (%)	98.66
Fines (0.425 < d) (%)	1.32
D_{10} (mm)	0.13
D_{30} (mm)	0.39
D_{60} (mm)	0.85
Mean particle diameter (mm)	0.68
Coefficient of curvature (Cc)	1.38
Coefficient of uniformity (Cu)	6.54
USCS Class	SW

The grains are generally sub-angular to sub-rounded, reflecting a shape that is neither perfectly rounded) nor sharply angular. This indicates that the grains exhibit slightly irregular but rounded edges, typical of standard quartz-based test sands as shown in Figure 2.

Figure 2 - Grain Size

2.1.2. Cement

The Portland cement used in the study was classified as Class I according to ASTM C150/C150M-21 [76] which is a standard specification for Portland cement. This classification indicates that the cement is suitable for general-purpose applications, such as in reinforced concrete construction, precast concrete products, and masonry. The specific gravity of the Portland cement was found to be 3.15. The Blaine fineness of the cement was measured to be 305 m^2/kg. The loss on ignition (LOI) of the cement was determined to be 2.1%. Table 3 shows the percentages of various chemical compounds that make up the Portland cement used in the study. It contains calcium oxide (CaO) and silicon dioxide (SiO_2) as its two highest chemical compounds, at 64.5% and 22.7%, respectively. Calcium oxide plays a crucial role in the cement hydration and silicon dioxide is a key component in the formation of the cementitious gel that binds the cement particles together.

Table 3 - Chemical composition of cement

Oxides (%)	**Cement (Type 1)**
CaO	64.5
SiO_2	22.7
Al_2O_3	4.8
Fe_2O_3	3.9
SO_3	1.4
MgO	0.3
K_2O	0.3
LOI	2.1

PREPRINT

2.2. Sample Preparation

Specimens for strength and stiffness testing were prepared under distinct preparation protocols compared to those designed for permeability evaluation. A comprehensive summary of molding and mix design variables (cement content, curing duration) is provided in Appendix A.

2.2.1. Sample Preparation for Strength (UCS) and Stiffness (G_0)

In order to test the strength and stiffness of the sand-cement mixture, 48 cylindrical-shaped samples were prepared. These samples had dimensions of 50 mm in diameter and 100 mm in height. The amount of soil required is calculated by using the dimensions of the mold. The radius is measured by using vernier caliper. Then to calculate the volume of the soil required, the height of soil in the mold is kept constant at 10 cm. Finally, by using the density relation, the mass of the soil sample has been calculated. In this study, two dry densities were targeted, which are 1.6 and 1.8 g/cm^3 to observe their impact on different properties such as strength and porosity. For each density, there were four cement percentages to be utilized. The cement

Table 4 - Details of cement content, test conducted, curing period and densities

Soil Type	Cement Content (%)	Molding Dry densities (g/cm^3)	Curing Period (days)	Test Type
Sandy Soil	1	1.6 and 1.8	0	Constant Head Test
	3		0	Constant Head Test
	6		0	Constant Head Test
	10		0	Constant Head Test
	1		4	Constant Head Test and UCS
	3		4	Constant Head Test and UCS
	6		4	Constant Head Test and UCS
	10		4	Constant Head Test and UCS
	1		7	Constant Head Test and UCS
	3		7	Constant Head Test and UCS
	6		7	Constant Head Test and UCS
	10		7	Constant Head Test and UCS
	1		28	UCS
	3		28	UCS
	6		28	UCS
	10		28	UCS

PRE-PRINT

percentages were 1%, 3%, 6% and 10% of the dry weight of sand as shown in Table 4. These percentages, guided by preliminary trials and established studies in literature [31,34,77,78], were designed to identify the minimum cement dosage required to ensure cohesive integrity (i.e., prevent sample disaggregation). Lower cement contents (e.g., 1&3%) represent threshold values for maintaining structural stability in lightly stabilized sands, whereas higher dosages (6&10%) reflect typical ranges for load-bearing applications. After the mass of each component of a mix has been calculated, the cement and sand were dry mixed together thoroughly using a mechanical mixer for a period of five minutes to ensure that they were homogeneously blended. To prepare the samples for testing, the split mold has been used to create cylindrical-shaped samples. To prepare the sand-cement mixture for testing, the dry mixture was poured into a mold in three equal layers. After each layer, an equal amount of water was added to the mixture. The process was repeated for each layer, ensuring thorough wetting and achieving the desired consistency. Wet tamping was used to compact the soil, enhancing its strength and stability. The samples were carefully removed from the mold to prevent any damage or deformation. Then, the samples were transferred to a humidity chamber where they were placed under controlled conditions of 24 ± 2 °C and relative humidity of about 95% as indicated by ASTM C511–03 [79] for a period of 4, 7, and 28 days. The purpose of this curing process is to ensure that the samples reach the desired strength and to stabilize the material for further testing.

2.2.2. Sample Preparation for Permeability

A total of 24 samples were carefully prepared in order to investigate the permeability of the soil-cement mixture (ACS), as shown in Table 4. The amount of soil required is calculated by using dimensions of the permeameter. The radius is measured by using vernier caliper. Then to calculate the volume of the soil required, the height of soil in the mold is kept constant at 20 cm. Finally, by using the density relation the mass of soil sample has been calculated. The soil sample with the higher density (1.8 g/cm^3) required compaction to maintain the 20 cm height, whereas the soil sample with the lower density (1.6 g/cm^3) only needed minimal or no compaction. Four different compositions were made, each with a different amount of cement (1%, 3%, 6%, and 10%). Two soil samples with densities of 1.8 g/cm^3 and 1.6 g/cm^3 were used for each cement percentage. To make the samples, exact amounts of sandy soil and cement were carefully mixed together. The mixture was divided into three equal portion and then poured into molds with a standard 8 cm diameter and 20 cm height. After pouring each layer the compaction was applied for 1.8 g/cm^3. The mixture was distributed evenly to make sure it covered the final outlet. The specimens were then subjected to curing for 0, 4, and 7 days, respectively. The samples were saturated throughout this procedure as water was introduced from the top. A number of constant head permeability tests performed in accordance with ASTM D2434 [80] guidelines were required for the permeability. Notably, the average of the previous three measurements was used to calculate each sample's hydraulic conductivity.

2.2.3. Testing Regime

Following sample preparation and curing, a number of tests were conducted to evaluate the samples' properties and characteristics, including UCS, UPV, and Constant Head tests.

PREPRINT

2.2.4. Unconfined Compressive Strength

The unconfined compressive strength (UCS) of the cemented soil samples was determined following ASTM D1633-00 [81]. The test is carried out by subjecting a cylindrical sample to a uniaxial compressive load without any lateral confinement. Prior to testing, specimens were removed from the humidity chamber, and their weight, height, and diameter were measured. A PC-controlled load frame (23 kN capacity,0.005 kN precision) was employed to apply a uniaxial compressive load at a constant axial displacement rate of 1 mm/min, compliant with ASTM D2166-16 [82], to ensure controlled strain and reproducible failure. The load was applied to the specimen's top platen while the bottom remained fixed, with real-time monitoring of load and vertical displacement. Testing continued until specimen failure (defined by post-peak load reduction or 15% axial strain), and the maximum load at failure was recorded. Pressure (stress) was measured via a calibrated load cell that converted axial force into electrical signals, while deformation (strain) was tracked using a displacement transducer (e.g., LVDT or optical encoder) monitoring vertical movement. Real-time data from these sensors were transmitted to a PC interface, which displayed live stress-strain curves during testing. Upon test completion, the peak stress (UCS) was recorded, and stress-strain plots were generated for analysis. The setup, as shown in Figure 3, highlights key components including the load cell, transducer, and control board.

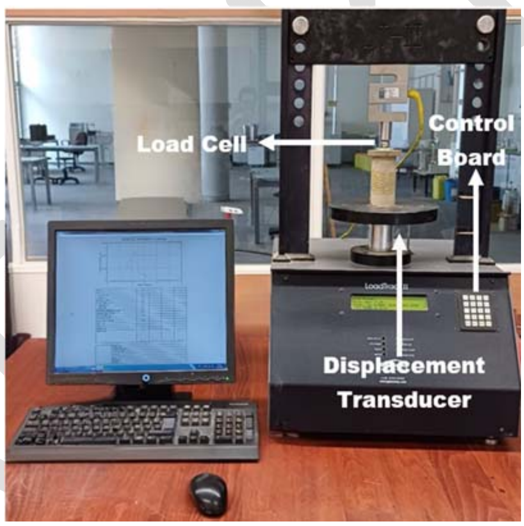

Figure 3 - Testing setup for UCS

To ensure reliability, three replicate specimens per mix design were tested, and the average UCS value was reported, with outliers (>10% deviation) excluded.

2.2.5. Pulse Velocity Tests (Pundit)

The maximum shear modulus (G_0) of cemented sand specimens was calculated using ultrasonic pulse velocity (UPV) testing, adhering to the ASTM C597-02 standard [83]. A

Pundit device (MATEST Ultrasonic Tester Model C368) was employed, utilizing paired transducers: one emitting a shear wave and the other receiving it as shown in Figure 4. Transducers were affixed to opposite sides of the specimen and silicon grease was applied on both ends of specimen to ensure optimal acoustic coupling. Adequate pressure was applied to eliminate air gaps and stabilize wave transmission. The transmitting transducer generated a shear wave, and the receiver recorded the travel time through the sample. Shear wave velocity (V_s) was derived from this transit time, enabling calculation of the maximum shear modulus (G_0)

The shear wave velocity (V_s) obtained from the test enables the calculation of the maximum shear modulus (G_0) using the specimen's density (ρ), as expressed in Equation (1).

$$G_0 = \rho * (V_s)^2 \tag{1}$$

where, the dry density (ρ) of the cemented sand was predetermined during sample preparation, with values set at either 1.6 g/cm^3 or 1.8 g/cm^3. The non-destructive UPV method is frequently integrated with complementary mechanical tests, such as UCS evaluations, to establish reliable, standardized correlations for quantifying stiffness in cemented soils, as evidenced by numerous studies [84–87]. UPV and UCS tests aid in establishing empirical relationships between G_0 and UCS in cement-stabilized soils [88,89].

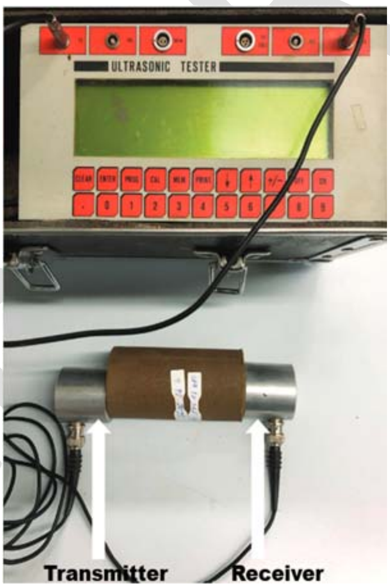

Figure 4 - Testing setup for UPV

2.2.6. Constant Head Test

The permeability of the cemented soil specimens was determined through the constant head permeability test, conducted in adherence to ASTM D2434 [80]. The permeameter apparatus, designed for this purpose, comprises four critical parameters: an inside diameter of 100 mm, a metal cylinder height accommodating the specimen, a piezometer length of 100 mm, and a specimen height of 20 cm. A cylindrical soil-cement samples of standardized dimensions (20 cm height × 10 cm diameter) were prepared and securely positioned within the permeameter. To ensure an airtight seal, a reinforced rubber ring was fastened atop the permeameter using stainless-steel screws, effectively isolating the specimen from external air ingress. By applying a vacuum, air is drawn out of the soil specimen. In the constant head test setup, a continuous water supply is necessary to achieve this, the inflow tube of the setup is connected to an upstream water tank. The tank provides a constant flow of water into the permeameter, which ensures that the hydraulic head remains constant throughout the test. Once the inflow is opened, water begins to flow through the permeameter and into the soil specimen. To measure the flow of water through the soil specimen, a beaker is used to collect the outflow volume. Once the system reached equilibrium, water was allowed to percolate through the specimen under the constant head condition.

To calculate the coefficient of permeability, the quantity of water discharged is measured (200 ml) over a specific time using a beaker placed at the outlet of the permeameter. The coefficient of water permeability (k) is calculated using Darcy's Law, which relates the flow rate of water through a porous medium to the properties of the medium and the hydraulic head gradient. Equation (2) is used to calculate the coefficient of permeability:

$$\mathrm{k} = \frac{\mathrm{QL}}{\mathrm{HAt}} \tag{2}$$

where k is the coefficient of permeability (cm/s); Q is the quantity of water discharged, (cm^3); L is the height of the soil specimen (cm); H is the constant head causing flow (cm); A is the cross-sectional area of the specimen(cm^2); and t is the time in seconds (s).

2.2.7. Runoff Coefficient Analysis

The Environmental Protection Agency (EPA) Storm Water Management Model (SWMM) is a widely used rainfall-runoff model for urban and suburban areas. It simulates runoff quantity and quality, including the evaluation of green infrastructure (GI) practices. SWMM, categorizes green infrastructure (GI) practices that capture runoff and provide detention, infiltration, and evapotranspiration as LID controls. SWMM allows for the representation of various GI/LID controls, such as bio-retention cells, rain gardens, green roofs, and permeable pavements, which capture and treat stormwater through infiltration, detention, and evapotranspiration methods as LID controls.

LID controls are designed to mimic the natural hydrologic processes that occur in undeveloped areas and can be represented by a combination of vertical layers with properties defined on a per-unit-area basis. This enables the use of LIDs of the same design but with different coverage areas to be applied in various sub-catchments of a study area. During a simulation, SWMM performs a moisture balance to track the movement of water between and within each LID layer.

The various layers used in LID controls include the Surface Layer, which corresponds to the ground or pavement surface that receives direct rainfall and generates surface outflow that either enters the drainage system or flows onto downstream land areas. In the literature

[90,91], the permeable pavement had a berm height of 25 mm, thickness of pavement layer of 60 mm, and thickness of storage layer of 250 mm. The thinner pavement layer and thicker storage layer are better for infiltration. Further, for small areas, it is recommended to use storage layer thickness between 150 mm to 450 mm [90,91]. The Pavement Layer, which is the layer of porous concrete or asphalt used in continuous permeable pavement systems. The Soil Layer, which is the engineered soil mixture used in bio-retention cells to support vegetative growth and can also be a sand layer placed beneath a pavement layer to provide bedding and filtration. The Storage Layer consists of a bed of crushed rock or gravel that provides storage in bio-retention cells, porous pavement, and infiltration trench systems, and for a rain barrel, it is simply the barrel itself. The Drain System conveys water out of the gravel storage layer and permeable pavement systems into a common outlet pipe or chamber as shown in Figure 2. These various layers in LID controls work together to manage stormwater runoff, improve water quality, and reduce the impact of development on the natural hydrologic cycle. In this study, pavement and storage layers are only considered as shown in Figure 5.

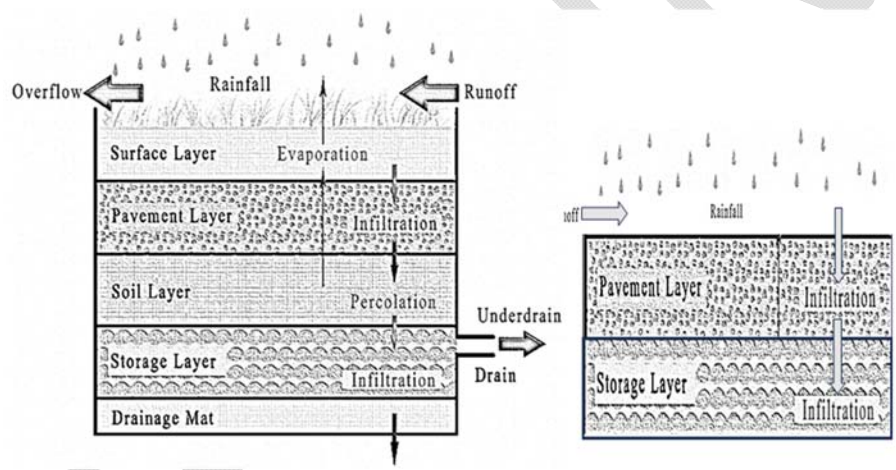

Figure 5 - LID layers used for SWMM modelling

The parameters and properties of different layers of LID are shown in Table 5 and Table 6, respectively. The void ratio and permeability for pavement layer depends on cement percentage used.

The Curve Number (CN) method, developed by the USDA NRCS in 1972 (US Soil Conservation Service, 1972), is used to calculate rainfall excess or effective rainfall from a rainfall event. It involves determining the infiltration amount by subtracting the rainfall excess from the total rainfall. The CN method relies on the CN value, which is determined by considering factors such as soil type, land use, vegetation, and other relevant characteristics. It represents the runoff potential and is used in the calculation of rainfall excess. The runoff (R) is given by Equation (3):

Table 5 - Different parameters of LID layers

Layer	Parameter	Units	Value
Surface Layer	Berm Height	mm	0
	Vegetation Volume Fraction		0
	Roughness		0.013
	Slope	%	2
Pavement Layer	Thickness	mm	150
	Void Ratio	Voids/Solids	*0.143
	Impervious Surface Fraction		0
	Permeability	mm/h	*28
Soil Layer	Thickness	mm	0
	Porosity	Volume Fraction	0
	Field Capacity	Volume Fraction	0
	Wilting Point	Volume Fraction	0
	Conductivity	mm/h	0
	Conductivity Slope	-	0
	Suction Head	mm	0
Storage layer	Thickness	mm	300
	Void Ratio	Voids/Solids	0.75
	Seepage Rate	mm/h	0
	Clogging Factor		0

*Depends on cement percentage used

Table 6 - Properties of LID area

Property	Unit	Value
Area of each unit	m^2	500
Number of units		1
% of Sub catchment occupied	%	100
Surface width per unit	m	20
% Initially saturated	%	0
% of pervious area treated	%	100
% of impervious area treated	%	0

PRE-PRINT

$$R = \frac{(P - 0.2S)^2}{(P + 0.8S)} \tag{3}$$

where R is the depth of direct runoff (mm). P is the depth of total rainfall (mm). S is a retention parameter known as depth of storage (mm) and derived from the CN value which is expressed as

$$S = \frac{25400}{CN} - 254 \tag{4}$$

The CN value is usually determined based on soil type, land use, and vegetation characteristics. However, it can also be calculated using Equations (3) and (4) if the infiltration or runoff amount for a rainfall event is known. In this study, the depth of infiltration and runoff was calculated using generated SWMM model. Then using S, the curve number is calculated.

3. RESULTS AND DISCUSSIONS

The effect of cement replacement on mechanical responses was discussed considering the UCS, UPV, and Constant Head tests. Additionally, Multifactorial Analysis of Cement Content, Curing Period and Density were studied with the aid of ANOVA method in this section. To form a bridge between the innovation and application, the practical application of artificially cemented sand was discussed in respect to mechanical findings.

3.1. Effect of Cement Replacement on Mechanical Response of Cement-Soil Mixture

3.1.1. Relative Density (D_r)

The observed trend showed that compacting soil-cement mixtures to higher dry densities significantly elevates relative density as shown in Figure 6. Elevated dry density (1.8 g/cm^3) exerts the most pronounced influence by fundamentally restructuring the soil matrix: higher compaction forces particles into closer proximity, minimizing initial void ratios and establishing a denser skeletal framework. This mechanical densification narrows the gap between the in-situ/dry density (ρ_d) and the material's theoretical maximum (ρ_{max}) as shown in Equation (5).

$$D_r = \frac{\rho_{max}(\rho_d - \rho_{min})}{\rho_d(\rho_{max} - \rho_{min})} \tag{5}$$

Where ρ_d is the achieved dry density of the specimen, ρ_{max} is the maximum dry density (densest state), and ρ_{min} is the minimum dry density (loosest state). As the dry density of the specimen (ρ_d) nears the maximum density (ρ_{max}), the difference (ρ_d-ρ_{min}) approaches the full range, pushing the relative density (D_r) toward 100%. This signifies a densely compacted state with negligible voids. Conversely, as ρ_d approaches the minimum density (ρ_{min}), D_r trends to 0%, reflecting loose, poorly compacted soil with high void content.

PRE-PRINT

Cement content amplifies this effect by introducing binding agents that occupy and bridge the residual voids. For instance, at 1.8 g/cm^3, increasing cement from 1% to 10% elevates D_r from 72.8% to 99.0% after 28 days, as surplus cement generates gels that infiltrate and stabilize the pre-compacted microstructure. However, this pore-filling efficacy is contingent on the initial density; at 1.6 g/m^3, larger voids persist, limiting cement's ability to bind particles cohesively (10% cement achieves only 44.5%). Curing time further refines D_r by enabling progressive hydration, as prolonged curing (4 to 28 days) allows cementitious reactions to mature, densifying the matrix through gradual void infilling. Critically, the interdependence of these factors is hierarchical: dry density establishes the increment in D_r, while cement content and curing time optimize the increment. The synergy is most evident in high-density systems (1.8 g/m^3), where compaction's rigid framework, combined with ample cement and extended curing, achieves near-full density (99%), as hydration products efficiently target confined micropores. Thus, while mechanical compaction governs the ceiling for achievable density, cementation and curing act as secondary refiners, collectively advancing D_r through physicochemical enhancement of the pre-optimized matrix.

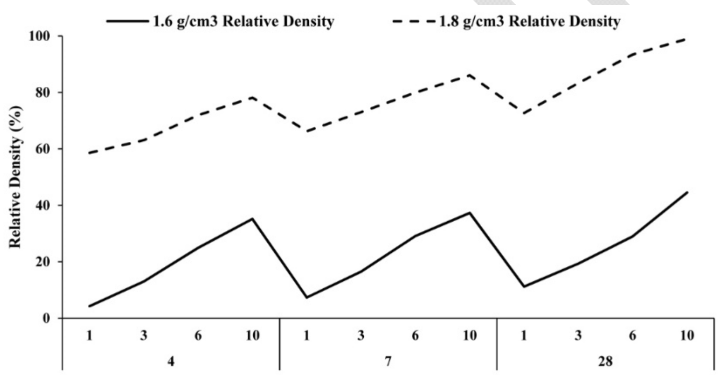

Figure 6 - Relative density of cement soil samples

3.1.2. Unconfined Compressive Strength (UCS)

The stress-strain behavior of cement-stabilized soils exhibits an enhancement in mechanical performance with increasing cement content, as demonstrated in Figure 7***Figure 7** - Stress-Strain behavior of best performing samples (high density, 1.8g/cm3 & long curing,28 days) at varying cement* for high-density (1.8 g/cm^3) and long-cured (28 days) specimens. Higher cement percentages, such as 10%, yield an elevated peak stress of 2,673 kPa, indicative of robust interparticle bonding and cohesive matrix formation, while lower percentages (1% and 3%) exhibit markedly reduced strengths of 26 kPa and 129 kPa, respectively. Concurrently, material stiffness intensifies with cement content, evidenced by steeper initial slopes of the stress-strain curves, which reflect diminished elastic deformation under load. Energy absorption, quantified by the area under the curve, also improves proportionally with cement content, underscoring the superior energy dissipation capacity of denser, well-cemented matrices. However, this mechanical enhancement introduces a critical trade-off in failure behavior: lower cement contents (1–3%) exhibit ductile responses, characterized by gradual post-peak strength degradation, whereas higher percentages (6–10%) transition to brittle failure, marked by abrupt fracture upon reaching peak stress. The study supports that higher cement content (via multiple CIPS flushes) elevated UCS but induced volumetric collapse and brittleness [92]. For instance, the 10% cement mix achieves the highest strength but fails abruptly, while the 3% mix retains residual load-bearing capacity despite lower peak values. To ensure statistical rigor, three specimens for each mix combination were tested, and peak strength values derived from individual stress-strain curves were averaged. These averaged values are synthesized in a newly plotted bar graph as shown in Figure 4, which visualizes strength trends across varying cement contents (1,3,6, and 10) %, densities (1.6 and 1.8 g/cm^3), and curing periods (4,7, and 28 days).

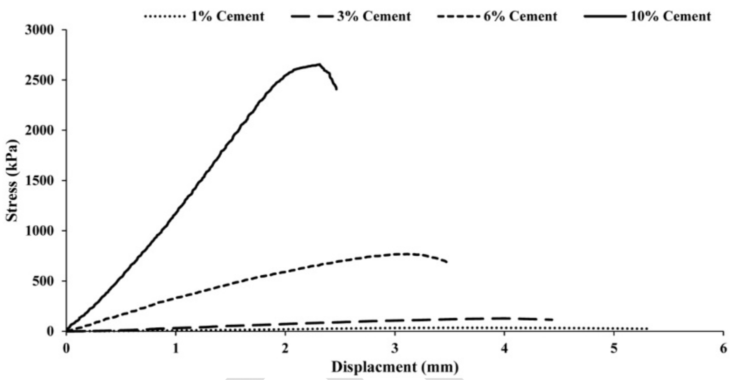

Figure 7 - Stress-Strain behavior of best performing samples (high density, 1.8g/cm^3 & long curing,28 days) at varying cement

Figure 8 demonstrates a consistent positive correlation between curing time and UCS of cemented sand, observed across all tested densities and cement contents. The progressive strength enhancement with extended curing periods underscores the critical role of hydration and pozzolanic reactions in developing cementitious bonds within the soil matrix. This trend aligns with findings from prior studies, which attribute strength gains to the progressive maturation of the stabilized soil's solid skeleton, governed by time-dependent hydration and pozzolanic reactions [50,93,94]. For specimens with low cement percentages (1&3%), UCS increases substantially during the initial curing (4 &7 days), followed by marginal gains from 7 to 28 days. This trend arises because limited cement availability restricts the hydration reaction, capping densification potential once early hydration reactions conclude. In contrast, higher cement contents (6–10%) sustain significant strength gains beyond 7 days, with UCS increasing between 7 and 28 days. The surplus cement enables prolonged hydration and pozzolanic reactions, fostering a denser and interconnected matrix. These findings align with established studies, which reported that the majority of hydration and pozzolanic reactions in cement-stabilized soils conclude within 28 days when sufficient cement is present, resulting in marginal strength gains thereafter [51,52,93,94]. Long-term observations corroborate that strength increments diminish significantly after 100 days [49], as hydration nears completion and reactive silica sources are depleted.

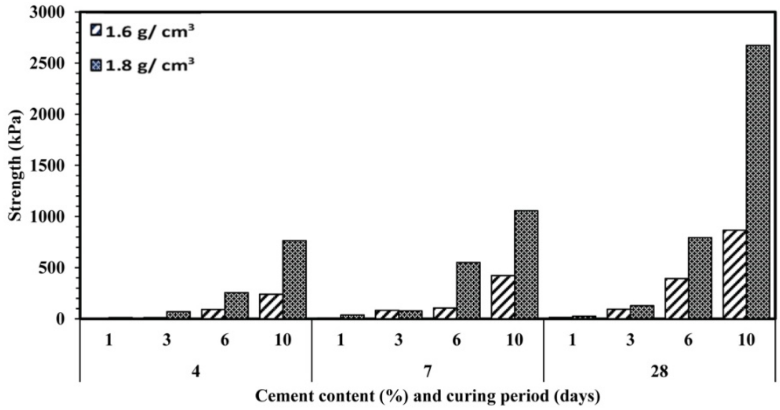

Figure 8 - Effect of different cement percentages and curing days on UCS

Figure 8 demonstrates a pronounced increase in UCS with rising cement content across all curing durations and densities. For instance, at a density of 1.8 g/cm^3 and 28 days of curing, UCS surged from 25 kPa (1% cement) to 2673 kPa (10% cement), reflecting a 100 times strength improvement. Similarly, Park [49] observed analogous behavior in cemented sands, reporting UCS increments from 155 kPa (2% cement) to 444 kPa (6% cement). Similarly, several studies confirm that increasing the cement content in cemented sand directly enhances its strength [31,34,39,41]. The increased strength of cement-stabilized soils arises from two key processes. First, when cement hydrates, it releases calcium hydroxide (CH), which chemically reacts with silica and alumina naturally present in the soil. These reactions produce calcium silicate hydrate (C-S-H) and calcium aluminate hydrate (C-A-H) gels, which act as a binding agent, bonding soil particles together. Second, over time, these gels expand and harden into a rigid, interlocking network, similar to concrete that fills voids between soil particles and consolidates them into a unified, cohesive mass [42–46,50]. The strength of cement-stabilized soils increases with higher cement content but exhibits diminishing returns beyond a critical threshold. For instance, in 1.8 g/cm^3 samples cured for 28 days, raising cement from 3% to 6% amplifies strength by 6.2 times (129 kPa to 795 kPa), whereas increasing it further to 10% yields only a 3.4 times gain (795 kPa to 2,673 kPa). This trend aligns with findings from prior studies, which confirm that while higher cement content initially enhances UCS significantly by filling voids and forming cementitious bonds, incremental gains diminish beyond a threshold [58,59,95].This trend arises because, at lower cement levels (≤6%), added binder effectively fills voids and bonds particles, creating a cohesive matrix. However, beyond ~6%, voids become saturated, limiting space for new cementitious gels to form, and excess cement may coat particles instead of bonding them, reducing efficiency. Additionally, water availability constraints can leave surplus cement unreacted.

Figure 8 demonstrates a consistent positive correlation between dry density and UCS in cement-stabilized soils. For instance, at 6% cement content and 4 days of curing, specimens compacted to 1.8 g/cm^3 exhibit a UCS of 256.7 kPa, compared to 92.6 kPa for those at 1.6 g/cm^3, highlighting a nearly threefold strength improvement. This trend persists across all cement percentages and curing durations as higher density reduces porosity and enhances particle packing, fostering a denser matrix with fewer voids. Compacted soils (e.g., 1.8 g/cm³) exhibit improved interparticle contact and more efficient cementation, as hydration products form more efficiently between tightly packed grains, creating a continuous, load-bearing network. Experimental studies consistently show that UCS in stabilized soils increases with dry density. Huang and Airey [54]demonstrated that both UCS and stiffness of artificially cemented carbonate sand improved with higher dry unit weights (13, 16, and 19 kN/m^3) and increased gypsum cement content (5–20%). However, the impact of cementation diminished at the highest densities, due to pore saturation. Similarly, Consoli et al. [31] observed that UCS increased as the density rose from 17.3 kN/m^3 to 19.7 kN/m^3 with increasing cement content (1, 2, 3, 5, and 7%). Moreover, research conducted at a fixed cementation reagent concentration (0.25 M CCR) confirmed that enhanced packing improves UCS, with values of 98, 141, and 160 kPa recorded for loose, medium, and dense states, respectively [96].

3.1.3. Shear Modulus (G_0)

The shear modulus (G_0), derived from ultrasonic pulse velocity (UPV) testing, exhibits trends similar to UCS, increasing proportionally with cement content, curing duration, and dry density. As illustrated in Figure 9, G_0 rises significantly with higher cement content, reflecting enhanced stiffness and mechanical performance. For instance, increasing cement from 6% to 10% amplifies G_0 across all curing periods and dry densities. This behavior mirrors UCS trends, as hydration products densify the matrix, reduce porosity, and improve interparticle bonding.

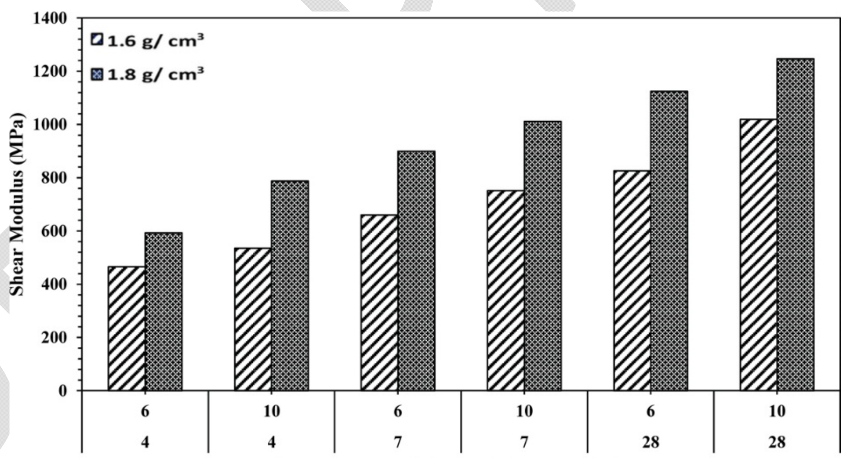

Figure 9 - Effect of cement content on stiffness of samples

The shear modulus (G_0) of cemented sands is profoundly influenced by curing duration, as evidenced by progressive stiffness gains over time. For specimens at 1.6 g/cm^3 density, increasing the curing period from 4 to 28 days elevates G_0 from 465 MPa to 825 MPa (77% increase) for 6% cement content, and from 535 MPa to 1,020 MPa (91% increase) for 10%

cement content. Density further enhances G_0 by optimizing particle packing and stress transfer. At 6% cement and 7 days curing, raising density from 1.6 to 1.8 g/cm^3 boosts G_0 from 660 MPa to 900 MPa, demonstrating compaction's role in minimizing voids and improving interparticle contact. Similarly, at 1.6 g/cm^3 and 28 days curing, increasing cement from 6% to 10% elevates G_0 from 825 MPa to 1,020 MPa, as surplus binder fosters denser gel networks.

Prior studies consistently corroborate the observed relationship between G_0, binder content, density, and curing time, reinforcing the validity of the current findings. For instance, increasing gypsum cement content (5,10&20%) and dry unit weight ((13,16&19 kN/m³) in artificially cemented carbonate sand enhances both UCS and stiffness [54]. The maximum shear modulus (G_0) rises with higher cement content (2,4,6&8%) due to intensified cementitious bonding [97]. Atkinson and Coop [98] highlighted that cementation shifts critical state lines and normal compression behavior, increasing shear modulus. Complementary research on lime-stabilized dispersive soils further validated these trends, revealing that G_0 follows a power-law relationship with lime dosage and compaction density, while extended curing (7 to 60 days) amplifies stiffness via prolonged pozzolanic reactions [99]. These studies collectively emphasize that hydration products and pore refinement drive G_0 enhancement, with higher binder content and density optimizing interparticle bonding [54,97,99].

3.1.4. Permeability

The permeability response of cement-stabilized soils was systematically evaluated via constant head permeability tests, as illustrated in Figure 10. Results demonstrate a consistent reduction in the coefficient of permeability (k) with increasing cement content, dry density, and curing duration.

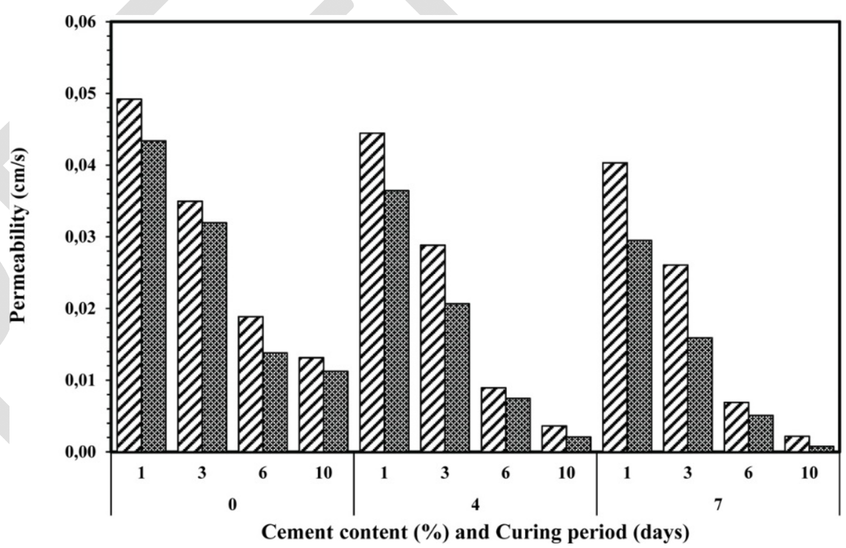

Figure 10 - Effect of different cement percentages and curing days on Permeability

The experimental data in Figure 10 reveals a consistent inverse relationship between cement content and permeability, irrespective of curing time and density. As cement content increases incrementally from 1% to 10%, the coefficient of permeability (k) decreases significantly, reaching near-zero values especially at 10% cement after 7 days of curing. Each incremental rise in cement content enhances void-filling efficiency, effectively blocking fluid pathways and transforming the soil into a quasi-impermeable material. For example, at a constant density (1.8 g/cm^3) and curing (7 days), increasing cement content from 1% to 10% reduces k from 2.95×10^{-2} cm/s to 8.0×10^{-4} cm/s. This trend is consistent with findings from a study on cemented sand-gravel, which reported a similar permeability decline when cement content increased from 0 to 12.5% over a 14-day curing period [41]. Permeability exhibits a nonlinear inverse correlation with cement content, where higher binder percentages lead to substantial reductions initially, but the rate of decrease diminishes progressively, a trend widely corroborated by other researchers [41,55,56]. Initial cement increments (from 1% to 3%) moderately reduce permeability by partially filling larger pores, though the limited binder quantity cannot fully occupy these dominant flow pathways. Intermediate additions (from 3% to 6%) yield the most significant improvements, as sufficient cement generates abundant hydration products to block smaller pores and disrupt interconnected flow networks, drastically lowering permeability. However, higher cement additions (6% to 10%) showed diminishing reductions by filling residual pores, particularly in high-density or long-cured specimens, ensuring ultra-low permeability. Lower cement contents partially fill intra-aggregate voids, slightly reducing permeability, while higher dosages extend to inter-aggregate spaces, forming a denser microstructure and significantly lowering permeability [57,60,61].

For samples with identical cement content, extended curing periods consistently reduce permeability, reflecting progressive pore refinement through hydration, as shown in Figure 10. For example, a specimen with 1.6 g/cm^3 density and 6% cement exhibits a permeability decrease from 1.89×10^{-2} cm/s (0 days) to 8.9×10^{-3} cm/s (4 days) and further to 6.9×10^{-3} cm/s (7 days), as prolonged hydration fills residual voids and strengthens the soil matrix, systematically lowering hydraulic conductivity. A study on cement-stabilized dredged sediment (CDS) confirms that prolonged curing reduces permeability. The decline in k from 7 to 28 days was more pronounced at higher cement contents, indicating a strong correlation between curing duration and cement dosage [62]. Similarly, a study on soils mixing cement (soilcrete) reported a reduction in permeability by several orders of magnitude over a 120-day curing period, reinforcing the relationship between extended curing and decreased hydraulic conductivity [60]. As curing progresses, cement hydration refines the pore structure, reducing large pores and increasing small ones, which reduces permeability [62,63,100]. The experimental data further reveals a strong inverse correlation between compacted density and permeability in cement-stabilized soils, with higher-density samples (1.8 g/cm^3) consistently exhibiting lower permeability compared to lower-density counterparts (1.6 g/cm^3) under identical curing and cement conditions as shown in Figure 5. This trend is statistically robust (R^2=0.768), indicating that 76.8% of permeability variability is attributable to density differences. Higher density reduces permeability by minimizing pore connectivity and enhancing particle packing, which obstructs fluid flow pathways [64]. Further, a study on compacted soils treated with cement showed that an increase in compaction level (from 85% to 105% of the maximum dry density) led to a significant decrease in permeability [101]. The combined effect of curing time and dry density on permeability is complex: while prolonged curing generally reduces permeability, its impact is more pronounced in high-density soils. Study on cement-treated clayey soils confirm that permeability declines most sharply in denser matrices subjected to extended curing, as hydration products refine the already optimized pore structure [102].

3.2. Multifactorial Analysis on Influence of Cement Content, Curing Period and Density on Mechanical Parameters

This study employed a multifactor ANOVA (5% significance level) to systematically evaluate the influence of cement content (1%, 3%, 6%, 10%), curing duration (0, 4, 7, 28 days), and dry density (1.6, 1.8 g/cm^3) on the mechanical and hydraulic properties of cemented soil. These variables were selected to assess their impact on UCS, k, and G_0. The analysis identified statistically significant relationships between the independent variables (cement content, curing duration, density) and dependent parameters (UCS, permeability, shear modulus), both individually and through their interactions. These findings are robustly supported by *p*-values < 0.05, indicating less than 5% probability that the observed correlations occurred by chance under the null hypothesis of no association. The statistical analysis, as showcased in Table 6, shed light on the crucial variables such as UCS, G_0, and k of cemented sand. To understand the intricate relationships between these variables and the mechanical parameters, various tests, such as mean square (measure of variance attributed to factors versus random error) and F-ratio (comparison of factor-induced variance to random variance, determining significance), were employed. These tests allowed for meaningful comparisons, enabling a deeper understanding of the specific effects and significance of each variable on the strength and behavior of the cemented sand.

The ANOVA results reveal a pronounced distinction between mechanical (UCS, G_0) and hydraulic (*k*) properties of cemented sand. Cement content exhibits a dominant influence on strength and stiffness, with substantial mean square values of 1,220,000 (UCS) and 45,000 (G_0), reflecting its critical role in forming cementitious bonds. In contrast, its impact on permeability is minimal (mean square = 0.0015), as permeability depends more on pore structure than bonding. Similarly, density and curing days show higher mean square values for mechanical properties (704,613 and 422,937 for UCS; 50,063 and 186,000 for G_0) compared to permeability (0.00016 and 0.0004), underscoring their stronger association with particle packing and hydration maturity than pore connectivity. These disparities highlight that while cement content drives strength/stiffness, density and curing are pivotal for permeability reduction.

The corrected F-Ratio values clarify that cement content and density exert a stronger statistical influence on mechanical properties (UCS: F=19.5, G_0: F=20.4; density: UCS F=74.3, G_0: F=22.7) compared to permeability (F=2.9 and F=3.05, respectively). In contrast, curing days disproportionately affect permeability (F=7.7) over G_0 (F=11.3, *F*=11.3) and UCS (F=6.8, *F*=6.8). This indicates that while cement and density dominantly enhance strength and stiffness through particle bonding and compaction, curing primarily refines pore structure to reduce permeability.

PRE-PRINT

Table 7 - Two-way ANOVA analysis summary table

	Source	Sum of Squares	Df	Mean Square	F-Ratio	P-Value
	MAIN EFFECTS					
Unconfined Compressive Strength (UCS)	A: Cement (%)	3670000	3	1220000	19.55	0.0017
	B: Curing Days	845875	2	422937	6.76	0.0291
	C: Density (g/cm^3)	704613	1	704613	11.25	0.0153
	INTERACTIONS					
	AB	1150000	6	192108	3.07	0.0991
	AC	934507	3	311502	4.98	0.0457
	BC	153361	2	76680.6	1.22	0.3581
	RESIDUAL	375642	6	62607		
	TOTAL (CORRECTED)	7840000	23			
	MAIN EFFECTS					
Shear Modulus (G_0)	A: Cement (%)	45000	1	45000	20.4	0.0457
	B: Curing Days	37200	2	186000	74.29	0.0117
	C: Density (kg/m^3)	50063.2	1	50063.2	22.69	0.0414
	INTERACTIONS					
	AB	1510	2	757	0.34	0.7445
	AC	58.4	1	58.4	0.03	0.8857
	BC	482	2	241	0.11	0.9016
	RESIDUAL	4413.23	2	2206.62		
	TOTAL (CORRECTED)	473527	11			
	MAIN EFFECTS					
Permeability (k)	A: Cement (%)	0.00453	3	0.00151	2.9722	0
	B: Curing Days	0.000785	2	0.000393	7.733	0.0001
	C: Density (g/cm^3)	0.000155	1	0.000155	3.047	0.0015
	INTERACTIONS					
	AB	0.000150608	6	0.00000251	4.94	0.0364
	AC	0.0000237	3	0.00000789	1.55	0.295
	BC	0.0000169	2	0.00000843	1.66	0.2668
	RESIDUAL	0.0000305	6	0.00000507		
	TOTAL (CORRECTED)	0.00568902	23			

PREPRINT

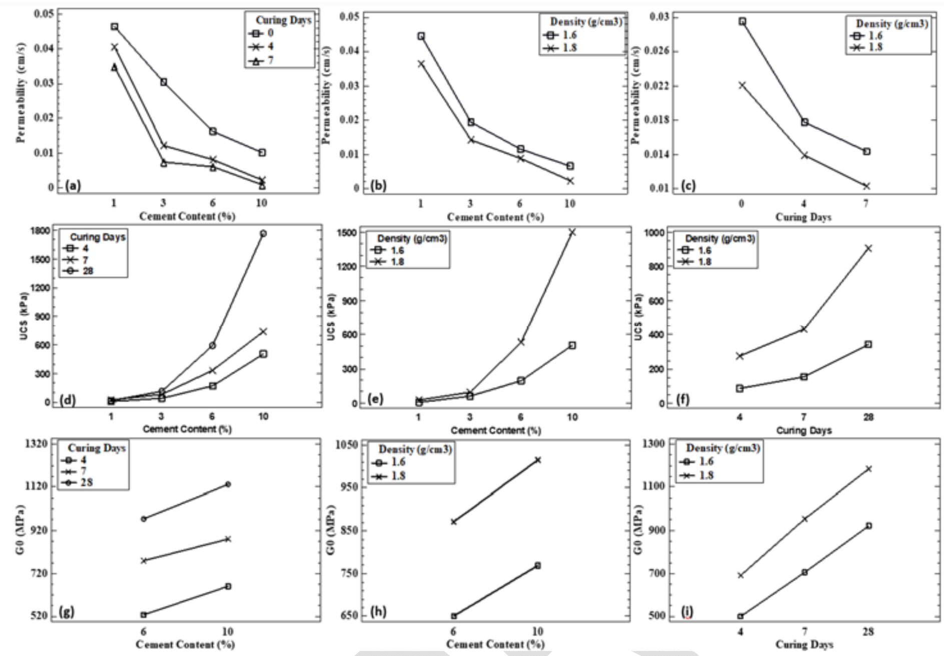

Figure 11 - Visual representation of effect of different independently variables on dependent varibles

Figure 11 presents a visual representation of the relationship between the independent variables (dry density, curing time, and cement content) and the dependent parameters (UCS, shear modulus, and permeability coefficient). The figure provides a comprehensive understanding of the complex connections and highlights the influence that the independent variables have on the measured parameters. By examining the graph, insights such as changes in the independent variables affect the values of the dependent parameters can be observed. Higher strength and shear modulus values have been observed at higher densities, with a notable decrease in permeability at higher densities as shown in Figure 11 (c, f and i). These findings indicate that increasing the density of the material leads to improved strength characteristics while simultaneously reducing the permeability. On the other hand, as the cement content increases, there is a general trend of increasing strength and shear modulus while decreasing permeability as shown in Figure 11 (a, d and g). However, a notable finding is that the decrease in permeability is more pronounced when the cement content increases from 1% to 3% compared to the subsequent increases from 3% to 6% and 6% to 10%. This suggests that the initial increase in cement content has a more significant impact on reducing permeability, while further increases beyond a certain threshold may have diminishing effects. Moreover, increases in the curing period (from 0 to 7 days) have been found to contribute to a decrease in permeability and an increase in strength and shear modulus as shown in Figure 11 (a, d and g).

4. RUNOFF CONTROL ANALYSIS OF ARTIFICIALLY CEMENTED SAND

Table 7 shows the output data from a Storm Water Management Model (SWMM) simulation with Low Impact Development (LID) control for a specific precipitation event with an intensity of 330 mm/hr. A portion of the rainwater resulted in runoff and was discharged as surface runoff. Additionally, some of the rainwater was stored in the system, as indicated by the total storage columns. Without considering evaporation and infiltration losses, the focus is primarily on the inflow and outflow of water within the system, as well as the storage capacity. As it provides insights into the response of the cemented sand system to the precipitation event and the ability to retain and release water. The coefficient of permeability was calculated using constant head test and void ratio for each sample was calculated assuming the soil was saturated. For each mix these parameters were provided to the software to get the output.

The sample identifier 1.6,0D,3C represents a specific sample in the dataset, where 1.6 indicates the density in g/cm^3, 0D represents the curing period of 0 days, and 3C represents the cement percentage of 3%. Upon examining Table 7**,** a clear trend emerges where the surface outflow increases while the storage decreases with an increase in the percentage of cement. For example, comparing the samples with the same density (1.6 g/cm^3) and curing period (4 days) but varying cement percentages, it can be observed that the surface runoff rises from 162.95 mm to 199.00 mm, while the storage decreases from 167.05 mm to 141.92 mm. This pattern suggests that a higher cement content contributes to a greater surface runoff, as indicated by the increased surface outflow. Additionally, the reduction in storage implies a diminished capacity to retain water within the system.

These observations indicate that a higher percentage of cement hinders water infiltration and promotes runoff from the surface. Further, the relationship between cement percentage and its impact on runoff and infiltration is not straightforward and follows a non-linear pattern. The gradual increase in the curve number value from 1% to 6% cement content suggests that adding more cement in this range has a relatively smaller effect on reducing infiltration and increasing surface runoff. However, beyond a cement percentage of 6, there is a rapid increase in the curve number value, indicating that further increases in cement content significantly decrease infiltration capacity and result in increased surface runoff. This observation has implications for understanding and managing water in cemented soil systems. It suggests that there is a threshold point (around a cement content of 6%) beyond which the increase in cement content has a more pronounced impact on the hydrological response. The comparison between the two samples, having the same curing period (4 days) and cement content (10%) but with different densities (1.8 g/cm^3 and 1.6 g/cm^3) reveals that the higher density of 1.8 results in a significantly higher curve number such as a CN number of 86. This implies that the higher density sample has a greater tendency for runoff and lower capacity for water infiltration compared to the sample with lower density. Despite having the same curing period and cement content, the higher curve number of the 1.8 g/cm^3 sample indicates that density plays a more significant role in influencing the hydrological response, leading to reduced infiltration and increased runoff potential.

PREPRINT

Table 8 - Runoff coefficient analysis using SWMM

Total Inflow (P)	Runoff (R)	Total Storage (S)	Sample ID	CN	Strength	Permeability Coefficient (k)	Void ratio (e)
mm	mm	mm	#		(kPa)	mm/hr.	
330	166.46	163.54	1.6,0D,1C	61	n/a	1771.3	0.304
330	166.90	163.10	1.6,0D,3C	61	n/a	1258.5	0.299
330	167.89	162.11	1.6,0D,6C	61	n/a	679.1	0.288
330	171.62	158.38	1.6,0D,10C	62	n/a	544.8	0.248
330	162.95	167.05	1.6,4D,1C	60	4.77	1600.2	0.345
330	169.26	160.74	1.6,4D,3C	61	12.32	497.8	0.273
330	169.91	160.09	1.6,4D,6C	61	92.60	322.0	0.266
330	199.00	141.92	1.6,4D,10C	64	240.50	130.6	0.252
330	166.72	163.28	1.6,7D,1C	61	8.79	1451.6	0.301
330	171.91	158.09	1.6,7D,3C	62	83.06	326.6	0.245
330	175.19	154.81	1.6,7D,6C	62	206.40	248.8	0.212
330	296.00	36.83	1.6,7D,10C	87	422.85	34.3	0.154
330	172.49	157.51	1.8,0D,1C	62	n/a	1562.1	0.239
330	176.01	153.99	1.8,0D,3C	62	n/a	934.8	0.204
330	177.90	152.10	1.8,0D,6C	63	n/a	496.5	0.186
330	181.19	148.81	1.8,0D,10C	63	n/a	188.2	0.156
330	166.20	163.80	1.8,4D,1C	61	12.76	1312.0	0.307
330	172.01	157.99	1.8,4D,3C	62	69.90	384.6	0.244
330	175.70	154.30	1.8,4D,6C	62	256.70	269.2	0.205
330	291.00	42.25	1.8,4D,10C	86	765.65	38.5	0.164
330	168.62	161.38	1.8,7D,1C	61	37.28	1062.3	0.280
330	176.32	153.68	1.8,7D,3C	62	78.69	213.1	0.301
330	178.55	151.45	1.8,7D,6C	63	552.80	183.0	0.180
330	302.00	30.33	1.8,7D,10C	89	1057.55	27.9	0.143

It is noteworthy that the samples with higher curve numbers also exhibit higher strength. However, it is important to highlight that these samples may not be suitable for permeable pavement applications. While higher strength is desirable for various applications, permeable pavements prioritize water infiltration and drainage. The increased curve number, indicating reduced infiltration potential, suggests that these samples may not effectively allow water to permeate through the pavement surface and contribute to stormwater runoff. The sample with a dry density of 1.8 g/cm^3, a curing period of 7 days, and a cement content of 6% with a curve number of 63 and a strength value of 552.8 kPa emerges as a well-balanced choice that

PREPRINT

considers both strength and permeability (infiltration). While it may not boast the highest strength among the samples or the lowest curve number indicating high permeability, it strikes a favorable equilibrium between these two factors. A curve number of 63 indicates that the sample will behave similarly to a good grass cover condition [103]. It suggests that the sample has a moderate capacity for infiltration and water storage, allowing a significant portion of rainfall to infiltrate into the underlying soil rather than contributing to runoff. This behavior is desirable in stormwater management, as it helps to reduce the volume and peak discharge of surface runoff, promoting natural groundwater recharge and minimizing the risk of urban flooding.

The trend observed in the permeability is characterized by a decrease in values as the cement content, curing periods, and density increase. The aforementioned findings indicate that a higher concentration of cement, an extended duration of curing, and enhanced particle packing result in a more compact and less porous material, thereby reducing the connectivity of pores and fluid flow. Finally, it can be inferred from the shear modulus values that an increase in cement content, longer curing periods, and higher density typically result in rise of stiffness and greater resistance to shearing forces. The observed phenomenon can be ascribed to the augmentation of interparticle bonding and optimization of packing, leading to the development of a more rigid substance with an elevated shear modulus.

5. CONCLUSION

This study examined various factors such as cement content, curing period, and sample dry density to understand their influence on the strength and permeability of the cemented soil. Here are some key findings from this study:

There is a positive correlation between curing time and the strength of the cement mixture. Longer curing periods generally result in increased strength. Increasing the percentage of cement in the mixture tends to result in higher strength, but the relationship is not linear. Higher cement percentages (6%,10%) contribute to increased strength, but there are diminishing returns. For lower cement percentages (1% and 3%), the strength increases significantly from 4 days to 7 days of curing but shows only modest increases from 7 days to 28 days. Higher cement percentages (6% and 10%) continue to show significant strength increases even after 7 days of curing. The density of the material also influences its strength. Increasing the density generally leads to higher strength, as a higher density results in a more compact and less porous material with better particle interlocking and stronger bonding.

Increasing the amount of cement in the mixture generally leads to lower permeability values, indicating reduced water flow through the cemented soil. The decrease in permeability is more significant when increasing the cement percentage from 6% to 10% compared to increasing it from 3% to 6%. Higher cement content can fill voids between aggregates, creating a more compact and dense material, thereby reducing permeability. Longer curing periods generally result in decreased permeability. As the cement hydrates and solidifies during curing, the resulting material becomes denser and less porous, leading to lower permeability values. Higher sample densities result in lower permeability. A higher density leads to a more compact and less porous material, reducing the spaces through which fluids can flow.

PRE-PRINT

Higher cement percentages in cemented soil have a non-linear impact on runoff and infiltration during rainfall events. Increasing cement content beyond approximately 6% significantly reduces infiltration capacity and promotes surface runoff. The density of the samples also plays a crucial role in the hydrological response. Higher density samples have reduced infiltration potential and increased runoff potential, as indicated by higher curve numbers. Furthermore, samples with higher curve numbers and reduced infiltration potential exhibit higher strength. However, these samples may not be suitable for permeable pavements that prioritize water infiltration and drainage. To strike a favorable balance between strength and permeability (infiltration capacity), samples with a dry density of 1.8 g/cm^3, a curing period of 7 days, and a cement content of 6% are recommended.

In conclusion, the comprehensive ANOVA conducted in this study revealed significant relationships between the independent variables (cement content, curing days, and sample dry density) and the dependent variables (unconfined compressive strength, permeability coefficient, and shear modulus) in cemented soil. The analysis showed that cement content had a substantial impact on unconfined compressive strength and shear modulus, with a relatively weaker influence on permeability. Dry density and curing days had stronger effects on strength-related properties compared to permeability. The F-ratios supported these findings, indicating that cement content had a greater influence on permeability, while curing days and density had relatively more pronounced effects on permeability compared to strength-related properties. The graphical representation revealed important insights into the relationships between the independent variables and dependent parameters. Increasing cement content generally led to decreased permeability, with a more significant effect observed when going from 1% to 3%. However, further increases in cement content showed diminishing effects on permeability. Higher curing days and cement percentages contributed to reduced permeability and increased strength. Additionally, higher sample densities were associated with higher strength values and a decrease in the permeability coefficient.

In summary, this study highlights that a balance between strength and permeability can be achieved with a cement content of 6%, a dry density of 1.8 g/cm^3, and a curing period of 7 days. These conditions optimize strength while maintaining moderate permeability, making them suitable for applications requiring both durability and controlled water infiltration.

Data Availability

All data and models that support the findings of this study are available from the corresponding author upon reasonable request.

References

[1] J. Huang, A.E. Hartemink, Soil and environmental issues in sandy soils, (2020). https://doi.org/10.1016/j.earscirev.2020.103295.

[2] A. Bruand, C. Hartmann, G. Lesturgez, Physical properties of tropical sandy soils : a large range of behaviours, (2005).

PREPRINT

[3] J.G. Bockheim, A.E. Hartemink, J. Huang, Distribution and properties of sandy soils in the conterminous USA – A conceptual thickness model, and taxonomic analysis, Catena (Amst) 195 (2020) 104746. https://doi.org/10.1016/J.CATENA.2020.104746.

[4] M. Shahbazi, M. Rowshanzamir, S.M. Abtahi, S.M. Hejazi, Optimization of carpet waste fibers and steel slag particles to reinforce expansive soil using response surface methodology, Appl Clay Sci 142 (2017) 185–192. https://doi.org/10.1016/J.CLAY.2016.11.027.

[5] E.C. Brevik, A.E. Hartemink, Early soil knowledge and the birth and development of soil science, Catena (Amst) 83 (2010) 23–33. https://doi.org/10.1016/J.CATENA.2010.06.011.

[6] C. McDowell, stabilization of soils with lime, lime-flyash, and other lime reactive materials, Highway Research Board Bulletin (1959).

[7] R. Eires, A. Camões, S. Jalali, Ancient Materials and Techniques to Improve the Earthen Building Durability, Key Eng Mater 634 (2015) 357–366. https://doi.org/10.4028/WWW.SCIENTIFIC.NET/KEM.634.357.

[8] C. Kelley, durability and maintenance of lime-stabilized bases, (1977).

[9] R.O. Abd-Al Ftah, B.A. Tayeh, K. Abdelsamie, R.D.A. Hafez, Assessment on structural and mechanical properties of reinforcement concrete beams prepared with luffa cylindrical fibre, Case Studies in Construction Materials 17 (2022) e01283. https://doi.org/10.1016/J.CSCM.2022.E01283.

[10] Y.I.A. Aisheh, D.S. Atrushi, M.H. Akeed, S. Qaidi, B.A. Tayeh, Influence of steel fibers and microsilica on the mechanical properties of ultra-high-performance geopolymer concrete (UHP-GPC), Case Studies in Construction Materials 17 (2022) e01245. https://doi.org/10.1016/J.CSCM.2022.E01245.

[11] L.K. Sharma, N.N. Sirdesai, K.M. Sharma, T.N. Singh, Experimental study to examine the independent roles of lime and cement on the stabilization of a mountain soil: A comparative study, Appl Clay Sci 152 (2018) 183–195. https://doi.org/10.1016/J.CLAY.2017.11.012.

[12] H. Verma, A. Ray, R. Rai, T. Gupta, N. Mehta, Ground improvement using chemical methods: A review, Heliyon 7 (2021) e07678. https://doi.org/10.1016/J.HELIYON.2021.E07678.

[13] I. Chang, M. Lee, A.T.P. Tran, S. Lee, Y.M. Kwon, J. Im, G.C. Cho, Review on biopolymer-based soil treatment (BPST) technology in geotechnical engineering practices, Transportation Geotechnics 24 (2020) 100385. https://doi.org/10.1016/J.TRGEO.2020.100385.

[14] H. Afrin, A Review on Different Types Soil Stabilization Techniques, Habiba Afrin. A Review on Different Types Soil Stabilization Techniques. International Journal of Transportation Engineering and Technology 3 (2017) 19–24. https://doi.org/10.11648/j.ijtet.20170302.12.

[15] F.A. Gidebo, H. Yasuhara, N. Kinoshita, Stabilization of expansive soil with agricultural waste additives: a review, International Journal of Geo-Engineering 14 (2023) 1–18. https://doi.org/10.1186/S40703-023-00194-X/TABLES/1.

PRE-PRINT

[16] M. Umar, K.A. Kassim, K.T. Ping Chiet, Biological process of soil improvement in civil engineering: A review, Journal of Rock Mechanics and Geotechnical Engineering 8 (2016) 767–774. https://doi.org/10.1016/J.JRMGE.2016.02.004.

[17] M. Patil, P.H. Dalal, S. Shreedhar, T.N. Dave, K.K.R. Iyer, Biostabilization techniques and applications in Civil Engineering: State-of-the-Art, Constr Build Mater 309 (2021) 125098. https://doi.org/10.1016/J.CONBUILDMAT.2021.125098.

[18] V. Rajoria, S. Kaur, a review on stabilization of soil using bio-enzyme, ijret: International Journal of Research in Engineering and Technology (n.d.) 2321–7308. http://www.ijret.org (accessed June 11, 2023).

[19] H. Verma, A. Ray, R. Rai, T. Gupta, N. Mehta, Ground improvement using chemical methods: A review, Heliyon 7 (n.d.) 7678. https://doi.org/10.1016/J.HELIYON.2021.E07678.

[20] D. Barman, S.K. Dash, Stabilization of expansive soils using chemical additives: A review, Journal of Rock Mechanics and Geotechnical Engineering 14 (2022) 1319–1342. https://doi.org/10.1016/J.JRMGE.2022.02.011.

[21] A.A. Firoozi, C. Guney Olgun, A.A. Firoozi, M.S. Baghini, Fundamentals of soil stabilization, International Journal of Geo-Engineering 8 (2017) 1–16. https://doi.org/10.1186/S40703-017-0064-9/FIGURES/3.

[22] A.A.S. Correia, P.D.F. Casaleiro, D.T.R. Figueiredo, M.S.M.R. Moura, M.G. Rasteiro, Key-Parameters in Chemical Stabilization of Soils with Multiwall Carbon Nanotubes, Applied Sciences 2021, Vol. 11, Page 8754 11 (2021) 8754. https://doi.org/10.3390/APP11188754.

[23] M.S. Abid, Stabilization of Soil using Chemical Additives, GRD Journal for Engineering | 1 (2016). www.grdjournals.com (accessed June 11, 2023).

[24] G.M. Bhatlawande, A.C. Babar, A.A. Darge, A Review on Different Methods of Soil Stabilization, International Journal of Engineering Science and Computing (2019). http://ijesc.org/ (accessed June 11, 2023).

[25] M. Laishram, D. Singh, S. Kumar, The Utilization of Industrial Waste as a Stabilizing Agent—A Review, Lecture Notes in Civil Engineering 281 (2023) 239–247. https://doi.org/10.1007/978-981-19-4731-5_22/TABLES/5.

[26] E. Zlatanović, N. Marinković, Z. Bonić, N. Romić, S. Djorić-Veljković, D. Cvetković, D. Djordjević, Comparative Study of the Effects of Conventional, Waste, and Alternative Materials on the Geomechanical Properties of Clayey Soil in the Chemical Soil Stabilisation Technique, Applied Sciences 2024, Vol. 14, Page 6249 14 (2024) 6249. https://doi.org/10.3390/APP14146249.

[27] J.B. Croft, The Influence of Soil Mineralogical Composition on Cement Stabilization, Https://Doi.Org/10.1680/Geot.1967.17.2.119 17 (2015) 119–135. https://doi.org/10.1680/GEOT.1967.17.2.119.

[28] Cement, Building Materials in Civil Engineering (2011) 46–423. https://doi.org/10.1533/9781845699567.46.

PREPRINT

[29] D. Marchon, R.J. Flatt, Mechanisms of cement hydration, Science and Technology of Concrete Admixtures (2016) 129–145. https://doi.org/10.1016/B978-0-08-100693-1.00008-4.

[30] H. Yang, Z. Qian, B. Yue, Z. Xie, Effects of Cement Dosage, Curing Time, and Water Dosage on the Strength of Cement-Stabilized Aeolian Sand Based on Macroscopic and Microscopic Tests, Materials 2024, Vol. 17, Page 3946 17 (2024) 3946. https://doi.org/10.3390/MA17163946.

[31] N.C. Consoli, D. Foppa, L. Festugato, K.S. Heineck, Key Parameters for Strength Control of Artificially Cemented Soils, Journal of Geotechnical and Geoenvironmental Engineering 133 (2007) 197–205. https://doi.org/10.1061/(ASCE)1090-0241(2007)133:2(197)/ASSET/12F5F147-8951-4DE1-9F0A-F5B3A38FD7E1/ASSETS/GRAPHIC/15.JPG.

[32] I. Shooshpasha, R.A. Shirvani, Effect of cement stabilization on geotechnical properties of sandy soils, Geomechanics and Engineering 8 (2015) 17–31. https://doi.org/10.12989/GAE.2015.8.1.017.

[33] S. Ahmad, O.S.B. Al-Amoudi, Y.M.H. Mustafa, M. Maslehuddin, M.H. Al-Malack, Stabilization and Solidification of Oil-Contaminated Sandy Soil Using Portland Cement and Supplementary Cementitious Materials, Journal of Materials in Civil Engineering 32 (2020). https://doi.org/10.1061/(ASCE)MT.1943-5533.0003169.

[34] N.C. Consoli, R.C. Cruz, M.F. Floss, Variables Controlling Strength of Artificially Cemented Sand: Influence of Curing Time, Journal of Materials in Civil Engineering 23 (2011) 692–696. https://doi.org/10.1061/(ASCE)MT.1943-5533.0000205/ASSET/E83D346D-BC59-489D-B3DB-D8BA079A05DA/ASSETS/IMAGES/LARGE/6.JPG.

[35] H. Choo, H. Nam, W. Lee, A practical method for estimating maximum shear modulus of cemented sands using unconfined compressive strength, J Appl Geophy 147 (2017) 102–108. https://doi.org/10.1016/J.JAPPGEO.2017.10.012.

[36] T.S. Amhadi, G.J. Assaf, G. Saygili, G. Loprencipe, Improvement of Pavement Subgrade by Adding Cement and Fly Ash to Natural Desert Sand, Infrastructures 2021, Vol. 6, Page 151 6 (2021) 151. https://doi.org/10.3390/INFRASTRUCTURES6110151.

[37] A.F. Cabalar, R.A. Omar, Stabilizing a silt using waste limestone powder, Bulletin of Engineering Geology and the Environment 82 (2023) 1–16. https://doi.org/10.1007/S10064-023-03302-4/FIGURES/21.

[38] A.F. Cabalar, Z. Karabash, Influence of Cement Type and Sample Preparation on the Small-Strain Behaviour of Sands, Arab J Sci Eng 44 (2019) 8835–8848. https://doi.org/10.1007/S13369-019-04070-8/FIGURES/21.

[39] T.S. Amhadi, G.J. Assaf, Strength and permeability potentials of cement-modified desert sand for roads construction purpose, Innovative Infrastructure Solutions 5 (2020) 1–10. https://doi.org/10.1007/S41062-020-00327-6/FIGURES/14.

PREPRINT

[40] H. Farshbaf Aghajani, H. Soltani-Jigheh, M. Salimi, S. Karimi, V. Estekanchi, R. Akbarzadeh Ahari, Investigating the strength, hydraulic conductivity, and durability of the CSG (cemented sand-gravel) check dams: a case study in Iran, SN Appl Sci 4 (2022) 1–19. https://doi.org/10.1007/S42452-022-05062-4/TABLES/6.

[41] H. Farshbaf Aghajani, H. Soltani-Jigheh, M. Salimi, S. Karimi, V. Estekanchi, R. Akbarzadeh Ahari, Investigating the strength, hydraulic conductivity, and durability of the CSG (cemented sand-gravel) check dams: a case study in Iran, SN Appl Sci 4 (2022) 1–19. https://doi.org/10.1007/S42452-022-05062-4/TABLES/6.

[42] S. Shahi, E. Fakhri, H. Yavari, S. Maleki Dizaj, S. Salatin, K. Khezri, Portland Cement: An Overview as a Root Repair Material, Biomed Res Int 2022 (2022) 3314912. https://doi.org/10.1155/2022/3314912.

[43] I.M. Padilla Espinosa, N. Barua, R. V. Mohan, Hydrostatic compression and pressure phase transition of major Portland cement constituents – Insights via molecular dynamics modeling, CEMENT 7 (2022) 100017. https://doi.org/10.1016/J.CEMENT.2021.100017.

[44] N. Arabi, N. Chelghoum, R. Jauberthie, L. Molez, Formation of C-S-H in calcium hydroxide-blast furnace slag-quartz-water system in autoclaving conditions, 27 (2015) 153–162. https://doi.org/10.1680/adcr.13.00069ï.

[45] M.J. McCarthy, T.D. Dyer, Pozzolanas and Pozzolanic Materials, Lea's Chemistry of Cement and Concrete (2019) 363–467. https://doi.org/10.1016/B978-0-08-100773-0.00009-5.

[46] E. John, T. Matschei, D. Stephan, Nucleation seeding with calcium silicate hydrate – A review, Cem Concr Res 113 (2018) 74–85. https://doi.org/10.1016/J.CEMCONRES.2018.07.003.

[47] F. Bell, Engineering Treatment of Soils, Engineering Treatment of Soils (1993) 235–245. https://doi.org/10.1201/9781482288971.

[48] N.C. Consoli, M.A. Vendruscolo, A. Fonini, F.D. Rosa, Fiber reinforcement effects on sand considering a wide cementation range, Geotextiles and Geomembranes 27 (2009) 196–203. https://doi.org/10.1016/J.GEOTEXMEM.2008.11.005.

[49] S.S. Park, Unconfined compressive strength and ductility of fiber-reinforced cemented sand, Constr Build Mater 25 (2011) 1134–1138. https://doi.org/10.1016/J.CONBUILDMAT.2010.07.017.

[50] J.R. Prusinski, S. Bhattacharja, Effectiveness of Portland Cement and Lime in Stabilizing Clay Soils, Transp Res Rec 1 (1999) 215–227. https://doi.org/10.3141/1652-28.

[51] K.A. Saeed, K.A. Kassim, H. Nur, Fizikalno-kemijska karakterizacija kaolinske gline s dodatkom cementa, Gradjevinar 66 (2014) 513–521. https://doi.org/10.14256/JCE.976.2013.

[52] S. Chaiyaput, N. Arwaedo, N. Kingnoi, T. Nghia-Nguyen, J. Ayawanna, Effect of curing conditions on the strength of soil cement, Case Studies in Construction Materials 16 (2022) e01082. https://doi.org/10.1016/J.CSCM.2022.E01082.

PREPRINT

[53] K.-S. Oh, T.-H. Kim, Dependence of the Material Properties of Lightweight Cemented Soil on the Curing Temperature, Journal of Materials in Civil Engineering 26 (2014). https://doi.org/10.1061/(ASCE)MT.1943-5533.0000940.

[54] J.T. Huang, D.W. Airey, Properties of Artificially Cemented Carbonate Sand, Journal of Geotechnical and Geoenvironmental Engineering 124 (1998) 492–499. https://doi.org/10.1061/(ASCE)1090-0241(1998)124:6(492).

[55] E. da S. Menger, M. Benetti, L. Festugato, L. da S. Ibeiro, R.D. Luza, Hydraulic Conductivity and Compressive Strength of Cemented Soils, Geotechnical and Geological Engineering 38 (2020) 6031–6039. https://doi.org/10.1007/S10706-020-01411-5/TABLES/4.

[56] F.C. Loch, O.J. Pejon, Study of Moisture and Cement Rates Influence on Hydraulic Conductivity of a Stabilized Sandy Soil by Means of a Factorial Design of Experiments, Engineering Geology for Society and Territory - Volume 5 (2015) 1333–1335. https://doi.org/10.1007/978-3-319-09048-1_254.

[57] N.D. Quang, J.C. Chai, Permeability of lime- and cement-treated clayey soils, Canadian Geotechnical Journal 52 (2015) 1221–1227. https://doi.org/10.1139/CGJ-2014-0134/ASSET/IMAGES/CGJ-2014-0134TAB7.GIF.

[58] F.C. Loch, O.J. Pejon, Study of Moisture and Cement Rates Influence on Hydraulic Conductivity of a Stabilized Sandy Soil by Means of a Factorial Design of Experiments, Engineering Geology for Society and Territory - Volume 5 (2015) 1333–1335. https://doi.org/10.1007/978-3-319-09048-1_254.

[59] J. Ji, G. Fan, Prediction of the permeability-reducing effect of cement infiltration into sandy soils, Water Supply 17 (2017) 851–858. https://doi.org/10.2166/WS.2016.183.

[60] B.T. Luong, H.-H. Tran-Nguyen, Investigation of Microstructure of Dredging Sand Mixing Cement Specimens to Interpret Reduction of Permeability, (2022) 157–166. https://doi.org/10.1061/9780784484012.016.

[61] X. Dong, X. Bao, H. Cui, C. Xu, X. Chen, Effects of Cement Treatment on Mechanical Properties and Microstructure of a Granite Residual Soil, Applied Sciences 2022, Vol. 12, Page 12549 12 (2022) 12549. https://doi.org/10.3390/APP122412549.

[62] S. Wang, X. He, G. Cai, L. Lang, H. Ma, S. Gong, Z. Niu, Investigation on Water Transformation and Pore Structure of Cement-Stabilized Dredged Sediment Based on NMR Technology, Materials 2022, Vol. 15, Page 3178 15 (2022) 3178. https://doi.org/10.3390/MA15093178.

[63] Z. Chong-hui, W. Zeng-hong, Experimental Research on the Variation Regularity of Permeability Coefficient of Cement Soil, Journal of Changjiang River Scientific Research Institute 30 (2013) 59. https://doi.org/10.3969/J.ISSN.1001-5485.2013.07.012.

[64] A. Sičáková, M. Kováč, Relationships between Functional Properties of Pervious Concrete, Sustainability 2020, Vol. 12, Page 6318 12 (2020) 6318. https://doi.org/10.3390/SU12166318.

[65] N.C. Consoli, F.D. Rosa, A. Fonini, Plate Load Tests on Cemented Soil Layers Overlaying Weaker Soil, Journal of Geotechnical and Geoenvironmental Engineering 135 (2009) 1846–1856. https://doi.org/10.1061/(ASCE)GT.1943-5606.0000158.

PREPRINT

[66] U.N.D. of E. and S. Affairs, World Population Prospects 2017 - Volume I: Comprehensive Tables, (2021). https://doi.org/10.18356/9789210001014.

[67] United Nations, World Population Prospects: The 2017 Revision | DESA Publications, (2017). https://desapublications.un.org/publications/world-population-prospects-2017-revision (accessed March 23, 2025).

[68] B.J. Hibbs, J.M. Sharp, Hydrogeological impacts of urbanization, Environmental and Engineering Geoscience 18 (2012) 3–24. https://doi.org/10.2113/GSEEGEOSCI.18.1.3.

[69] C.M. Liu, J.W. Chen, Y.S. Hsieh, M.L. Liou, T.H. Chen, Build sponge eco-cities to adapt hydroclimatic hazards, Handbook of Climate Change Adaptation (2015) 1997–2009. https://doi.org/10.1007/978-3-642-38670-1_91.

[70] C.E. Wilson, W.F. Hunt, R.J. Winston, P. Smith, Comparison of Runoff Quality and Quantity from a Commercial Low-Impact and Conventional Development in Raleigh, North Carolina, Journal of Environmental Engineering 141 (2015) 05014005. https://doi.org/10.1061/(ASCE)EE.1943-7870.0000842/ASSET/56E283CA-1032-4EC7-90C3-639912991EC4/ASSETS/IMAGES/LARGE/FIGURE8.JPG.

[71] M.E. Dietz, J.C. Clausen, Stormwater runoff and export changes with development in a traditional and low impact subdivision, J Environ Manage 87 (2008) 560–566. https://doi.org/10.1016/J.JENVMAN.2007.03.026.

[72] L.-M. Chen, J.-W. Chen, T.-H. Chen, T. Lecher, P.C. Davidson, Measurement of Permeability and Comparison of Pavements, (2019). https://doi.org/10.3390/w11030444.

[73] Low Impact Development (LID), (2000).

[74] S. Planning Roundtable, C. Bay Program, Prepared by the Prepared for the BETTER SITE DESIGN: A Handbook for Changing Development Rules in Your Community, (n.d.).

[75] U. Environmental Protection Agency, O. of Water, Stormwater Best Management Practice Permeable Pavements Minimum Measure: Post Construction Stormwater Management in New Development and Redevelopment Subcategory: Infiltration, (n.d.). https://www.epa.gov/npdes (accessed June 13, 2023).

[76] ASTM, ASTM C150/C150M-21: Standard Specification for Portland Cement, ASTM International D3699 (2021).

[77] N.C. Consoli, M.A. Vendruscolo, A. Fonini, F.D. Rosa, Fiber reinforcement effects on sand considering a wide cementation range, Geotextiles and Geomembranes 27 (2009) 196–203. https://doi.org/10.1016/J.GEOTEXMEM.2008.11.005.

[78] N.C. Consoli, F.D. Rosa, A. Fonini, Plate Load Tests on Cemented Soil Layers Overlaying Weaker Soil, Journal of Geotechnical and Geoenvironmental Engineering 135 (2009) 1846–1856. https://doi.org/10.1061/(ASCE)GT.1943-5606.0000158/ASSET/2A7E7EEB-7A9B-48CB-858D-E2AC303E7EF7/ASSETS/IMAGES/LARGE/15.JPG.

PRE-PRINT

[79] ASTM C511-03, Standard Specification for Mixing Rooms, Moist Cabinets, Moist Rooms, and Water Storage Tanks Used in the Testing of Hydraulic Cements and Concretes, American Society for Testing and Materials (2003).

[80] Test Method for Permeability of Granular Soils (Constant Head), (2022). https://doi.org/10.1520/D2434-22.

[81] ASTM International, ASTM D1633 - 00(2007) Standard Test Methods for Compressive Strength of Molded Soil-Cement Cylinders, ASTM International, West Conshohocken, PA, USA, (2007).

[82] Test Method for Unconfined Compressive Strength of Cohesive Soil, (2006). https://doi.org/10.1520/D2166-06.

[83] Test Method for Pulse Velocity Through Concrete, (2002). https://doi.org/10.1520/C0597-02.

[84] J. V. Kozubal, T. Kania, A.S. Tarawneh, A. Hassanat, R. Lawal, Ultrasonic assessment of cement-stabilized soils: Deep learning experimental results, Measurement 223 (2023) 113793. https://doi.org/10.1016/J.MEASUREMENT.2023.113793.

[85] W.S. Sarro, G.M. Assis, G.C.S. Ferreira, Experimental investigation of the UPV wavelength in compacted soil, Constr Build Mater 272 (2021) 121834. https://doi.org/10.1016/J.CONBUILDMAT.2020.121834.

[86] M. Hanafi, I. Javed, A. Ekinci, Evaluating the strength, durability and porosity characteristics of alluvial clay stabilized with marble dust as a sustainable binder, Results in Engineering 25 (2025) 103978. https://doi.org/10.1016/J.RINENG.2025.103978.

[87] L. Al-Subari, A. Ekinci, E. Aydın, The utilization of waste rubber tire powder to improve the mechanical properties of cement-clay composites, Constr Build Mater 300 (2021) 124306. https://doi.org/10.1016/J.CONBUILDMAT.2021.124306.

[88] N. Sathiparan, W.G.B.S. Jayasundara, K.S.D. Samarakoon, B. Banujan, Prediction of characteristics of cement stabilized earth blocks using non-destructive testing: Ultrasonic pulse velocity and electrical resistivity, Materialia (Oxf) 29 (2023) 101794. https://doi.org/10.1016/J.MTLA.2023.101794.

[89] J.A. Oke, H. Abuel-Naga, Assessment of a Non-Destructive Testing Method Using Ultrasonic Pulse Velocity to Determine the Compressive Strength of Rubberized Bricks Produced with Lime Kiln Dust Waste, Geotechnics 2023, Vol. 3, Pages 1294-1308 3 (2023) 1294–1308. https://doi.org/10.3390/GEOTECHNICS3040070.

[90] Y. Bai, Y. Li, R. Zhang, N. Zhao, X. Zeng, Comprehensive performance evaluation system based on environmental and economic benefits for optimal allocation of LID facilities, Water (Switzerland) 11 (2019). https://doi.org/10.3390/W11020341.

[91] T. Cui, Y. Long, Y. Wang, Choosing the LID for Urban Storm Management in the South of Taiyuan Basin by Comparing the Storm Water Reduction Efficiency, Water 2019, Vol. 11, Page 2583 11 (2019) 2583. https://doi.org/10.3390/W11122583.

[92] M.A. Ismail, H.A. Joer, M.F. Randolph, Sample Preparation Technique for Artificially Cemented Soils, Geotechnical Testing Journal 23 (2000) 171–177. https://doi.org/10.1520/GTJ11041J.

PREPRINT

[93] L. Zhang, Y. Li, X. Wei, X. Liang, J. Zhang, X. Li, Unconfined Compressive Strength of Cement-Stabilized Qiantang River Silty Clay, Materials 2024, Vol. 17, Page 1082 17 (2024) 1082. https://doi.org/10.3390/MA17051082.

[94] H.D. Do, V.N. Pham, H.H. Nguyen, P.N. Huynh, J. Han, Prediction of Unconfined Compressive Strength and Flexural Strength of Cement-Stabilized Sandy Soils: A Case Study in Vietnam, Geotechnical and Geological Engineering 39 (2021) 4947–4962. https://doi.org/10.1007/S10706-021-01805-Z/FIGURES/14.

[95] M.A. Ashraf, S.M.S. Rahman, M.O. Faruk, M.A. Bashar, Determination of Optimum Cement Content for Stabilization of Soft Soil and Durability Analysis of Soil Stabilized with Cement, American Journal of Civil Engineering 2018, Volume 6, Page 39 6 (2018) 39–43. https://doi.org/10.11648/J.AJCE.20180601.17.

[96] A.S. Muhammed, K. Kassim, M.U. Zango, C.S. Chong, Bio-cementation of Sandy Soil at different Relative Density, (2020).

[97] Y. Zhao Id, F. Qiao, F. Meng, Z. Zheng, J. Gu, H. Li, Experimental study on the effect of different cement content on the improvement of dynamic characteristics of seismic-prone poor soil, (2024). https://doi.org/10.1371/journal.pone.0300849.

[98] M.R. Coop, J.H. Atkinson, The mechanics of cemented carbonate sands, Geotechnique 43 (1993) 53–67. https://scholars.cityu.edu.hk/en/publications/the-mechanics-of-cemented-carbonate-sands(ce74debb-f7ae-4b71-831f-dcb463bff66c).html (accessed March 29, 2025).

[99] N.C. Consoli, R.A.Q. Samaniego, N.M.K. Villalba, Durability, Strength, and Stiffness of Dispersive Clay–Lime Blends, Journal of Materials in Civil Engineering 28 (2016). https://doi.org/10.1061/(ASCE)MT.1943-5533.0001632.

[100] T. Kunito, A. Honda, M. Mashima, S. Hamasato, A Study on the Relationship between Pore Structure and Coefficient of Permeability of Soil Stabilized with Cement, MRS Proceedings 137 (1988) 457–462. https://doi.org/10.1557/PROC-137-457/METRICS.

[101] H. Ranaivomanana, A. Razakamanantsoa, Toward a better understanding of the effects of cement treatment on microstructural and hydraulic properties of compacted soils, MATEC Web of Conferences 163 (2018) 06007. https://doi.org/10.1051/MATECCONF/201816306007.

[102] A. Abdallah, G. Russo, O. Cuisinier, Statistical and Predictive Analyses of the Strength Development of a Cement-Treated Clayey Soil, Geotechnics 2023, Vol. 3, Pages 465-479 3 (2023) 465–479. https://doi.org/10.3390/GEOTECHNICS3020026.

[103] CN Tables, (n.d.). https://www.hec.usace.army.mil/confluence/hmsdocs/hmstrm/cn-tables (accessed August 23, 2023).

PREPRINT

Appendix A

Table A-1 - Molding properties and mix design.

Soil Type	Sand Content (%)	Cement Content (%)	Molding Dry densities (g/cm^3)	Curing Period (Days)	Mass of sand (g)	Mass of Cement (g)	Mass of water (g)
Sand	99	1	1.6	4	311.157	3.143	125.14
Sand	97	3	1.6	4	304.871	9.429	125.14
Sand	94	6	1.6	4	295.442	18.858	125.14
Sand	90	10	1.6	4	282.870	31.430	125.14
Sand	99	1	1.6	7	311.157	3.143	125.14
Sand	97	3	1.6	7	304.871	9.429	125.14
Sand	94	6	1.6	7	295.442	18.858	125.14
Sand	90	10	1.6	7	282.870	31.430	125.14
Sand	99	1	1.6	28	311.157	3.143	125.14
Sand	97	3	1.6	28	304.871	9.429	125.14
Sand	94	6	1.6	28	295.442	18.858	125.14
Sand	90	10	1.6	28	282.870	31.430	125.14
Sand	99	1	1.8	4	350.036	3.536	89.43
Sand	97	3	1.8	4	342.964	10.607	89.43
Sand	94	6	1.8	4	332.357	21.214	89.43
Sand	90	10	1.8	4	318.214	35.357	89.43
Sand	99	1	1.8	7	350.036	3.536	89.43
Sand	97	3	1.8	7	342.964	10.607	89.43
Sand	94	6	1.8	7	332.357	21.214	89.43
Sand	90	10	1.8	7	318.214	35.357	89.43
Sand	99	1	1.8	28	350.036	3.536	89.43
Sand	97	3	1.8	28	342.964	10.607	89.43
Sand	94	6	1.8	28	332.357	21.214	89.43
Sand	90	10	1.8	28	318.214	35.357	89.43

PRE-PRINT